Electronic Supplementary Material (ESI) for Inorganic Chemistry Frontiers.

Supporting Information

Ligand-Regulated Photoinduced Electron Transfer within Metal–Organic Frameworks for Efficient Photocatalysis

Yang Tang[†], Guanfeng Ji[†], Hanning Li[†], Hui Gao[†], Cheng He[†], Liang Zhao[†]* and Chunying Duan[§]

[†]State Key Laboratory of Fine Chemicals, Frontier Science Center for Smart Materials, Dalian University of Technology, Dalian 116024, P. R. China.

[§]State Key Laboratory of Coordination Chemistry, Nanjing University, Nanjing 210093, P. R. China.

Table of Contents:

1. Materials and Methods

All the chemicals and solvents were of reagent grade quality obtained from commercial sources and used without further purification. *N*-((phenyl-D_5)methyl-D_2)pyrrolidine was synthesized using previously reported procedures[S1] and characterized by ^{1}H NMR. Co−**TBPA** was synthesized according to the methods in the reported literature[S2] and characterized by PXRD.

The elemental analysis of C, N, and H were performed on a Vario EL III elemental analyzer. FT-IR spectra were recorded from KBr pellets on ThermoFisher FT/IR-6700 instrument. The powder X-ray diffraction (PXRD) measurements were obtained on a Rigaku Smart Lab 9 kw X-ray diffractometer instrument with a Cu sealed tube in the angular range 2θ = 5−50° at 293 K. Thermogravimetric analyses were performed on a Mettler-Toledo TGA/SDTA-851 instrument and recorded under N_2 followed by a ramp of 10 °C·min^{-1} up to 800 °C. NMR spectra were measured on Bruker Vaian DLG-400, Bruker AVANCE Ⅲ 500 or Bruker Avance NEO 600M NMR spectrometers. ^{1}H NMR spectra were reported as follows: chemical shift (ppm, δ), multiplicity (s = singlet, d = doublet, t = triplet, q = quartet, m = multiplet, dd = double doublet, td = triple doublet), coupling constants (Hz), and numbers of protons. Liquid UV-Vis spectra were performed on a TU-1900 spectrophotometer. Solid UV-Vis and UV-Vis DRS spectra were recorded on Hitachi U-4100 UV-Vis-NIR spectrophotometer and a white standard of $BaSO_4$ was used as a reference. High-resolution mass spectra were collected on a Thermo Fisher Q Exactive Plus. Fluorescent spectra were recorded on Edinburgh FLS 920 stable/transient fluorescence spectrometer. Scanning electron microscopy (SEM) images were taken with JSM-7610F Plus Field Emission Scanning Electron Microscopy. Energy-dispersive X-ray spectroscopy (EDS) was taken with the JSM-7610F Plus Field Emission Scanning Electron Microscopy. X-ray photoelectron spectroscopy (XPS) signals were collected on a Thermo ESCALAB Xi+ spectrometer. Confocal laser scanning microscopy (CLSM) micrographs were collected by an Olympus Fluoview FV1000 instrument with λ_{ex} = 635 nm. The confocal and bright-field images of the obtained samples were scanned at λ_{em} = 655−755 nm and excited at 635 nm using a 405/488/635 nm filter.

Electrochemical impedance spectroscopy (EIS) measurements were measured on ZAHNER ENNIUM Electrochemical Workstation by using a three-electrode system with the sample-coated glassy carbon as the working electrode, platinum silk as a counter electrode, and an Ag/AgCl as a reference electrode. The 0.1 M Bu_4NPF_6 CH_3CN solution was used as the electrolyte. The sample (4.0 mg) was dispersed into 15.0 μL 5 wt% Nafion, 0.5 mL ethanol, and 0.5 mL H_2O mixed solution, and the working electrode was prepared by dropping the suspension onto the surface of the glassy carbon electrode. The working electrode was dried, and then EIS measurements were performed with a bias potential of 0.6 V.

Photoelectrochemical measurements were performed on a CHI 660E electrochemical workstation using a standard three-electrode system with 0.1 M Bu_4NPF_6 CH_3CN solution as the electrolyte. The sample-coated glassy carbon as the working electrode, platinum silk as a counter electrode, and Ag/AgCl as a reference electrode. The sample (4.0 mg) was dispersed into 15.0 μL 5 wt% Nafion, 0.5 mL ethanol, and 0.5 mL H_2O mixed solution. The working electrode was prepared by dropping the suspension onto the surface of the glassy carbon electrode. The photocurrent responses were measured at room temperature under the irradiation of a 420 nm LED which was purchased from the Beijing China Education Au-light Co., Ltd.

Mott-Schottky plots were measured on ZAHNER ENNIUM electrochemical workstation using a standard three-electrode system with 0.1 M Bu_4NPF_6 CH_3CN solution as the electrolyte. The sample-coated glassy carbon as the working electrode, platinum silk as a counter electrode, and Ag/AgCl as a reference electrode. The sample (4.0 mg) was dispersed into 15.0 μL 5 wt% Nafion, 0.5 mL ethanol, and 0.5 mL H_2O mixed solution. The working electrode was prepared by dropping the suspension onto the surface of the glassy carbon electrode.

We have employed the Vienna Ab initio Simulation Package (VASP) to perform all density functional theory (DFT) calculations.[S3-S6] The elemental core and valence electrons were represented by the projector augmented wave (PAW) method[S7] and plane-wave basis functions with a cutoff energy of 400 eV. Generalized gradient approximation with the Perdew-Burke-Ernzerh of (GGA-PBE) exchange-correlation functional was

employed in all the calculations.[S7-S8] Geometry optimizations were performed with the force convergency smaller than 0.05 eV/Å. The DFT+U approach was introduced to treat the highly localized Co 3d states, using parameters of U–J = 3.32 eV. All the atoms were relaxed in all the calculations. Monkhorst-Pack k-points of 1×1×1 were applied for all the calculations.

2. Preparation of Metal−Organic Frameworks

(1) Synthesis of 10-(4-bromophenyl)acridin-9(10*H*)-one (compound 1)

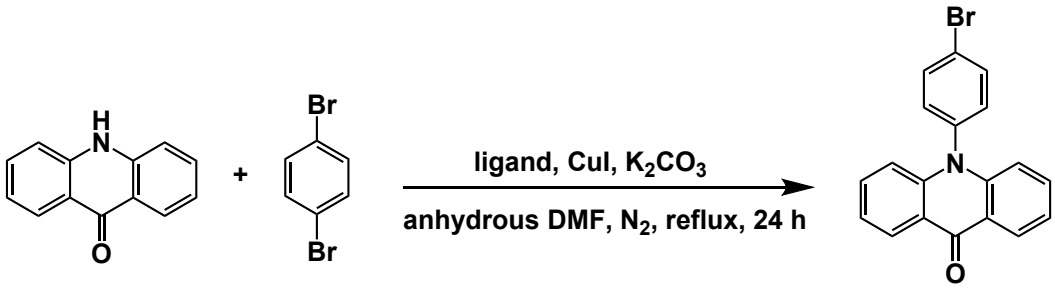

ligand = 2,2,6,6-tetramethyl-3,5-heptanedione

Compound 1 was synthesized using previously reported procedures[S9] and characterized by ^{1}H NMR.

(2) Synthesis of 2,7-dibromo-10-(4-bromophenyl)acridin-9(10*H*)-one (compound 2)

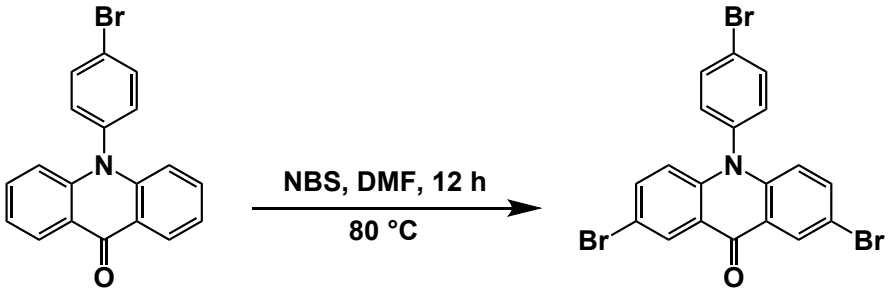

compound 1 compound 2

Compound 1 (1.00 g, 2.87 mmol) and *N*-bromosuccinimide (NBS) (1.53 g, 8.61 mmol) were dissolved in DMF (50 mL) and stirred at 80°C for 12 hours. Then, the mixture was quenched with water and CH_2Cl_2. After the separation of phases, the organic layer was washed with water (3 × 100 mL) and brine (1 × 100 mL), and dried over anhydrous Na_2SO_4. After filtering, the filtrate was evaporated to dryness under reduced pressure and the crude was purified by chromatography on silica gel using CH_2Cl_2 as the eluent to give compound 2 (Yield: 89%). ^{1}H NMR (500 MHz, $CDCl_3$) δ 8.58 (d, J = 2.4 Hz, 2H), 7.80 (d, J = 4.7 Hz, 2H), 7.51 (dd, J = 9.1, 2.4 Hz, 2H), 7.17 (d, J = 1.9 Hz, 2H), 6.57 (d, J = 9.1 Hz, 2H). ^{13}C NMR (126 MHz, $CDCl_3$) δ 175.66, 141.51, 137.23, 136.59, 134.80, 131.48, 129.89, 124.39, 123.01, 118.60, 115.69. HRMS (ESI^+): Calcd. for $[C_{19}H_{10}Br_3NO + H]^+$: m/z = 507.8365, Found: 507.8356. $[C_{19}H_{10}Br_3NO + Na]^+$: m/z = 529.8185, Found: 529.8172.

(3) Synthesis of dimethyl 4,4'-(10-(4'-(methoxycarbonyl)-[1,1'-biphenyl]-4-yl)-9-oxo-9,10-dihydroacridine-2,7-diyl)dibenzoate (compound 3)

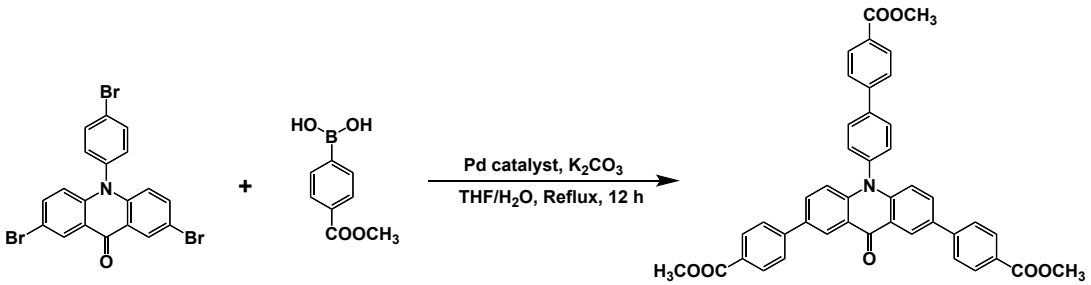

compound 2 compound 3

Compound 2 (1.00 g, 1.98 mmol), K_2CO_3 (1.64 g, 11.88 mmol), [1,1'-bis(diphenylphosphino)ferrocene]palladium(II) chloride (0.15 g, 0.20 mmol) and 4-(methoxycarbonyl)benzeneboronic acid (1.60 g, 7.92 mmol) were dissolved in a mixture containing 100 mL THF and 30 mL H_2O. The reaction mixture was refluxed with stirring for 24 hours under a nitrogen atmosphere, and then cooled to room temperature. The resulting mixture was poured into 100 mL of water and extracted with dichloromethane (3 × 100 mL). The organic phase was washed with water (2 × 100 mL) and dried over anhydrous Na_2SO_4. After filtering, the filtrate was evaporated to dryness under reduced pressure. The crude was purified by chromatography on silica gel using dichloromethane as the eluent to give compound 3 (Yield: 72%). ^{1}H NMR (500 MHz, $CDCl_3$): δ 8.78 (d, J = 2.2 Hz, 2H), 8.14 (d, J = 8.3 Hz, 2H), 8.04 (d, J = 8.3 Hz, 4H), 7.92 (d, J = 8.3 Hz, 2H), 7.77 – 7.71 (m, 4H), 7.67 (t, J = 7.1 Hz, 2H), 7.46 (d, J = 8.3 Hz, 1H), 6.90 – 6.86 (m, 1H), 3.91 (s, 1H), 3.86 (s, 1H). ^{13}C NMR (126 MHz, $CDCl_3$): δ 177.89, 166.88, 166.73, 143.92, 143.82, 142.69, 141.75, 138.47, 133.46, 132.18, 130.45, 130.43, 130.27, 130.05, 129.95, 129.01, 127.24, 126.74, 125.71, 122.12, 117.74, 52.27, 52.11. HRMS (ESI$^+$): Calcd. for $[C_{43}H_{31}NO_7 + H]^+$: m/z = 674.2173, Found: 674.2176. $[C_{43}H_{31}NO_7 + Na]^+$: m/z = 696.1993, Found: 696.1988.

(4) Synthesis of 4,4'-(10-(4'-carboxy-[1,1'-biphenyl]-4-yl)-9-oxo-9,10-dihydroacridine-2,7-diyl)dibenzoic acid (H_3**CDDA**)

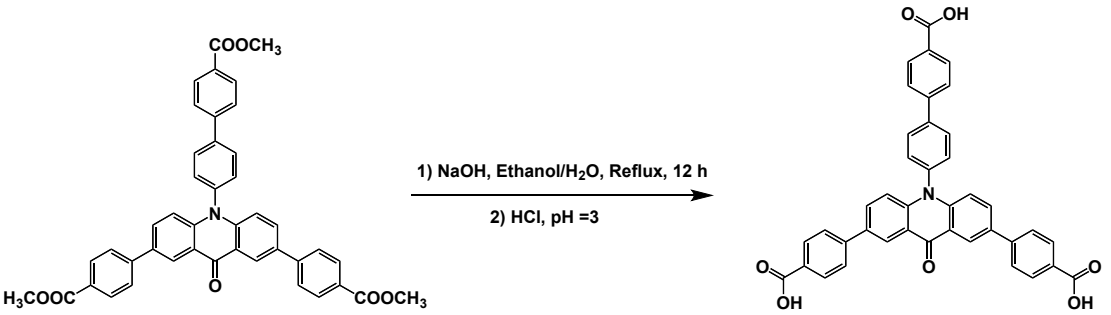

compound 3 H_3CDDA

Compound 3 (5.00 g, 7.43 mmol) and NaOH (4.40 g, 0.11 mol) were dissolved in a mixture containing 50 mL ethanol and 50 mL H_2O. The mixture was then refluxed for 24 hours. After cooling down to room temperature the mixture was acidified with HCl. The pH of the solution was adjusted to 3 to get a yellow precipitate. Finally, the precipitate was filtered and washed with plenty of water, dried in an oven to obtain the desired product (Yield: 90%). ^{1}H NMR (400 MHz, DMSO-d_6): δ 13.02 (s, 3H), 8.70 (d, J = 2.3 Hz, 2H), 8.19 (d, J = 8.4 Hz, 2H), 8.12 (d, J = 8.4 Hz, 1H), 8.09 – 8.04 (m, 3H), 8.02 (d, J = 8.4 Hz, 1H), 7.88 (d, J = 8.4 Hz, 4H), 7.77 (d, J = 8.4 Hz, 2H), 6.97 (d, J = 8.9 Hz, 2H). ^{13}C NMR (126 MHz, DMSO-d_6): δ 176.60, 167.06, 142.91, 142.86, 142.39, 140.49, 138.01, 132.45, 132.40, 130.52, 130.47, 130.33, 130.12, 130.08, 129.81, 129.63, 127.19, 126.50, 124.18, 121.36, 118.12. HRMS (ESI$^+$): Calcd. for $[C_{40}H_{24}NO_7]^-$: m/z = 630.1547, Found: 630.1554. Elemental analysis calcd for $C_{40}H_{25}NO_7$: C 76.05, H 3.99, N 2.22%. Found: C 76.07, H 4.04, N 2.18%.

(5) Preparation of Co−**CDDA**

A mixture of H_3**CDDA** (31.56 mg, 0.05 mmol) and $Co(OAc)_2{\cdot}4H_2O$ (10.45 mg, 0.055 mmol) was dissolved in water (0.5 mL) and *N*,*N*-dimethylformamide (DMF) (3 mL), which were placed in a 10 mL Teflon vessel within the autoclave. The mixture was heated at 120 °C for 72 hours and then cooled to room temperature at a rate of 3 °C h^{-1}. Red block crystals of Co−**CDDA** were obtained and collected from the mixture system above, washed with DMF and air-dried. Yield: 40% (based on the crystal dried under room temperature). Elemental analysis calcd for $C_{127.34}H_{83.49}Co_{5.10}N_{5.45}O_{27.44}$: C 62.91 H 3.44, N 3.14%. Found: C 63.28, H 3.26, N 3.32%. IR (KBr): 3400 (br, vs), 1606 (v), 1545 (w), 1520 (w), 1480 (m), 1400 (s), 1331 (m), 1300 (m), 1255 (m), 1106 (w), 1033 (w), 1006 (m), 991 (m), 1006 (m), 957 (w), 921 (m), 864 (m), 837 (w), 821 (m), 783 (s),

748 (m), 734 (m), 712 (m), 691 (m), 664 (m) cm^{-1} (Figure S9).

3. Single Crystal X-ray Crystallography

The intensities were collected on a Bruker SMART APEX CCD diffractometer equipped with a graphite-monochromated Mo-Kα (λ = 0.71073 Å) radiation source; the data were acquired using the SMART and SAINT programs.[S10,S11] The structure was solved by direct methods and refined by full matrix least-squares methods by the program SHELXL-2014.[S12] In the structural refinement of Co−**CDDA**, all the non-hydrogen atoms were refined anisotropically. Hydrogen atoms within the ligand backbones, DMF and the coordinate water molecules were fixed geometrically at calculated distances and allowed to ride on the parent non-hydrogen atoms. The three disordered benzene rings were refined with two parts while constraining the sum of the occupancies to unity. The relative occupancies of the two parts converged to values of 0.732 : 0.268; 0.816 : 0.174 and 0.626 : 0.374 respectively after refinement. To assist the stability of refinements, the disordered benzene rings were restrained as idealized regular polygons. The thermal parameters on adjacent atoms in benzene rings were restrained to be similar, respectively. The SQUEEZE subroutine in PLATON was used.[S13]

Table S1. Crystal data and structure refinements

Compound	Co−**CDDA**
Empirical formula	$C_{127.34}H_{83.49}Co_{5.10}N_{5.45}O_{27.44}$
Formula weight	2429.16
T / K	150(2)
Crystal system	triclinic
Space group	P-1
a / Å	22.6513(19)
b / Å	22.885(2)
c / Å	23.624(2)
α / °	66.092(2)
β / °	66.236(2)
γ / °	60.926(2)
V / Å^3	9453.7(14)
Z	2
D_{calcd} / g cm^{-3}	0.853
μ / mm^{-1}	0.485
F (000)	2486
Refl. collected / unique	286896 / 33235 [R_{int} = 0.1033]
Data / restraints / parameters	33235 / 1690 / 1690
Goodness-of-fit on F^2	1.129
$R[I>2\sigma(I)]$[a]	R_1 = 0.0819 wR_2 = 0.2523
R indices (all data)[b]	R_1 = 0.1242 wR_2 = 0.2681
$\Delta\rho_{max,min}$ / eÅ^{-3}	1.346 / -0.705
CCDC number	2263257

[a] $R_1 = \Sigma||F_o| - |F_c||/\Sigma|F_o|$; [b] $wR_2 = \Sigma[w(F_o^2 - F_c^2)^2]/\Sigma[w(F_o^2)^2]^{1/2}$

Table S2. Selected bond lengths (Å) for Co−**CDDA**

Bond	Length/Å	Bond	Length/Å
Co(01)-O(00K)	2.045(3)	Co(02)-O(00H)#2	2.048(4)
Co(01)-O(008)	2.077(3)	Co(02)-O(00O)#3	2.061(4)
Co(01)-O(009)	2.078(3)	Co(02)-O(00J)	2.061(4)
Co(01)-O(00G)	2.094(4)	Co(02)-O(00A)	2.075(3)
Co(01)-O(00M)	2.122(4)	Co(02)-O(00L)	2.098(4)
Co(01)-O(006)#1	2.141(3)	Co(02)-O(007)#1	2.223(3)
Co(03)-O(112)	1.81(3)	Co(04)-O(00D)	1.984(3)
Co(03)-O(012)	1.955(5)	Co(04)-O(008)	2.005(4)
Co(03)-O(010)	1.959(4)	Co(04)-O(00I)	2.027(4)
Co(03)-O(008)	1.995(3)	Co(04)-O(03K)#4	2.151(7)
Co(03)-O(00A)	1.999(4)	Co(04)-O(040)#4	2.230(5)
Co(05)-O(0)#5	1.89(3)	Co(05)-O(03H)#5	2.158(8)
Co(05)-O(00A)	1.995(4)	Co(05)-O(033)#5	2.238(6)
Co(05)-O(00N)#3	2.017(4)	Co(05)-O(04C)	2.258(7)
Co(05)-O(00P)#2	2.052(5)	O(006)-C(01E)	1.282(5)
N(00E)-C(014)	1.372(5)	O(007)-C(01E)	1.241(5)
C(00Q)-C(00X)	1.421(6)	C(00S)-H(00S)	0.9500
C(00R)-C(018)	1.375(6)	C(2)-C(1)	1.3900

Table S3. Selected bond angles (°) for Co−**CDDA**

Bond	Angle/°	Bond	Angle/°
O(00K)-Co(01)-O(008)	98.14(14)	O(00H)#2-Co(02)-O(00J)	93.55(16)
O(008)-Co(01)-O(009)	89.18(13)	O(00O)#3-Co(02)-O(00A)	95.59(15)
O(00K)-Co(01)-O(00G)	88.55(16)	O(00J)-Co(02)-O(00A)	172.26(16)
O(009)-Co(01)-O(00M)	175.13(14)	O(00J)-Co(02)-O(00L)	86.69(16)
O(00L)-Co(02)-O(007)#1	93.58(13)	O(012)-Co(03)-O(00A)	120.0(2)
O(112)-Co(03)-O(010)	108.8(11)	O(008)-Co(03)-O(00A)	98.73(13)
O(012)-Co(03)-O(008)	101.9(2)	O(00D)-Co(04)-O(008)	106.00(14)
O(00D)-Co(04)-O(040)#4	158.9(2)	O(008)-Co(04)-O(03K)#4	139.9(3)
O(00I)-Co(04)-O(040)#4	89.1(2)	O(008)-Co(04)-O(04D)	79.1(2)
O(03K)#4-Co(04)-O(040)#4	54.7(2)	O(00I)-Co(04)-O(04D)	172.9(3)
O(00D)-Co(04)-C(043)#4	130.0(3)	O(008)-Co(04)-C(043)#4	115.1(3)
O(00I)-Co(04)-C(043)#4	102.2(2)	O(03K)#4-Co(04)-C(043)#4	26.5(3)
O(04D)-Co(04)-C(043)#4	77.8(3)	O(040)#4-Co(04)-C(043)#4	29.0(2)
O(0)#5-Co(05)-O(00A)	119.6(14)	O(00N)#3-Co(05)-O(04C)	89.2(3)
O(00A)-Co(05)-O(00N)#3	113.36(15)	O(00N)#3-Co(05)-O(033)#5	156.1(2)
O(00P)#2-Co(05)-O(04C)	174.1(3)	O(00A)-Co(05)-O(04C)	80.0(3)
O(00N)#3-Co(05)-O(00P)#2	94.92(18)	O(03H)#5-Co(05)-O(033)#5	59.1(3)
O(00A)-Co(05)-O(03H)#5	145.6(3)	O(00N)#3-Co(05)-C(042)#5	128.7(4)
O(03H)#5-Co(05)-C(042)#5	31.6(5)	O(033)#5-Co(05)-O(04C)	90.6(3)
C(01E)-O(006)-Co(01)#7	122.0(3)	O(00A)-Co(05)-C(042)#5	116.5(4)
C(025)-O(009)-Co(01)	129.8(3)	Co(03)-O(008)-H(008)	104.5
C(02E)-O(00D)-Co(04)	125.4(3)	C(014)-N(00E)-C(01A)	119.2(3)
N(00F)-C(00Q)-C(01Q)	122.0(4)	C(018)-C(00R)-C(011)	120.1(4)
C(03D)-N(016)-C(03V)	122.1(4)	O(0)-C(9)-O(64)	119(3)
C(046)-O(012)-Co(03)	108.7(4)	C(031)-O(00H)-Co(02)#8	136.7(4)

4. Characterizations of Catalysts

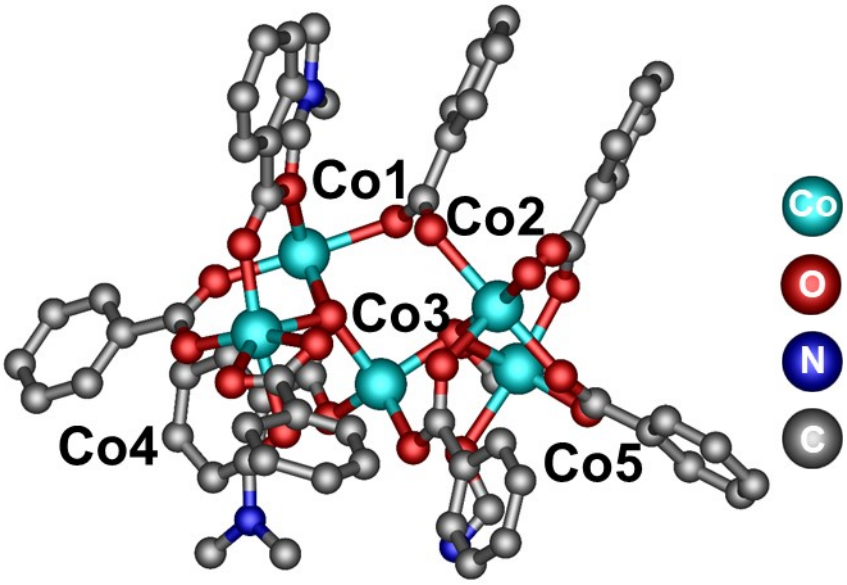

Figure S1. Coordination environments of Co ions in Co-**CDDA**.

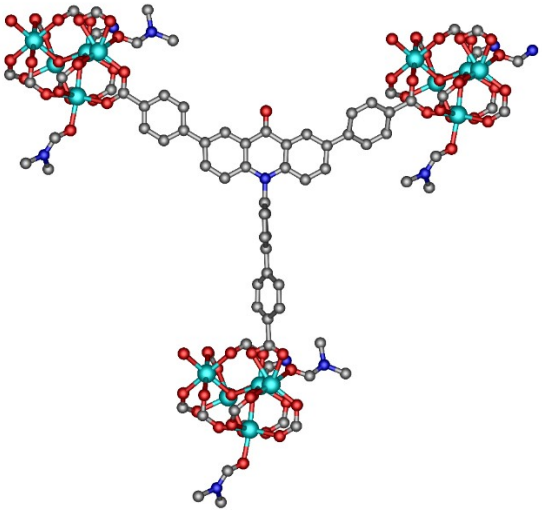

Figure S2. Each ligand of Co−**CDDA** connects with three Co_5 clusters.

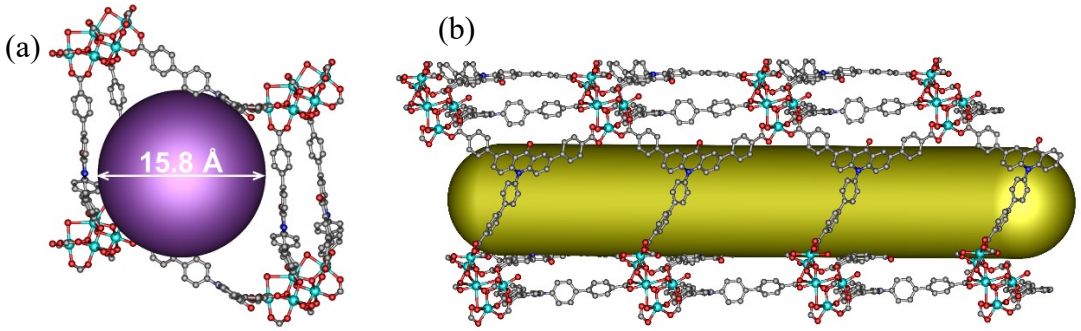

Figure S3. Pores of the 3D framework in Co−**CDDA** along the b direction (a) and c direction (b).

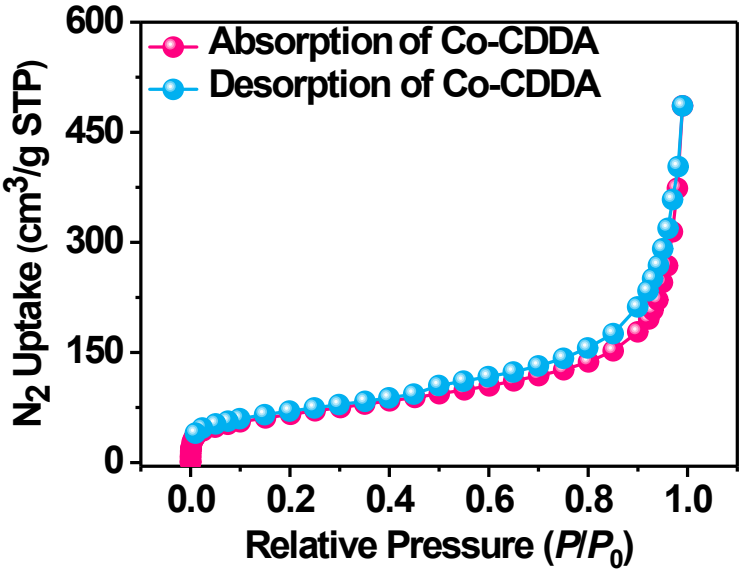

Figure S4. Nitrogen sorption isotherms for Co−**CDDA** at 77 K.

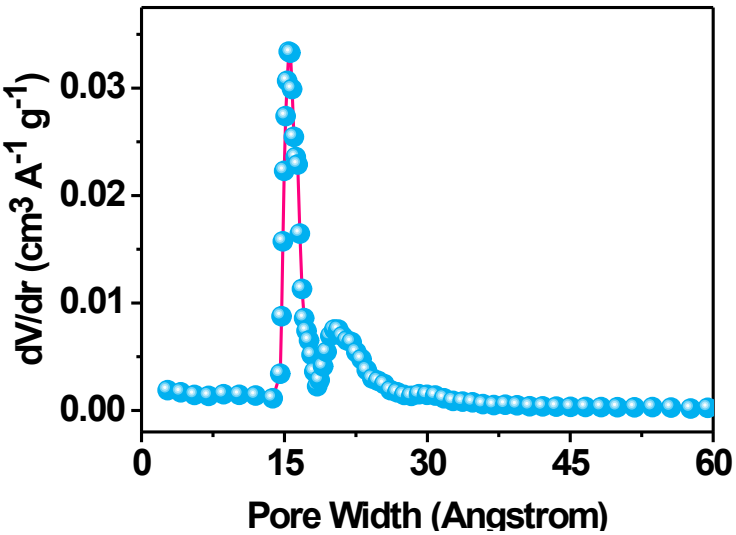

Figure S5. DFT pore size distribution for Co−**CDDA** using data measured with nitrogen at 77 K.

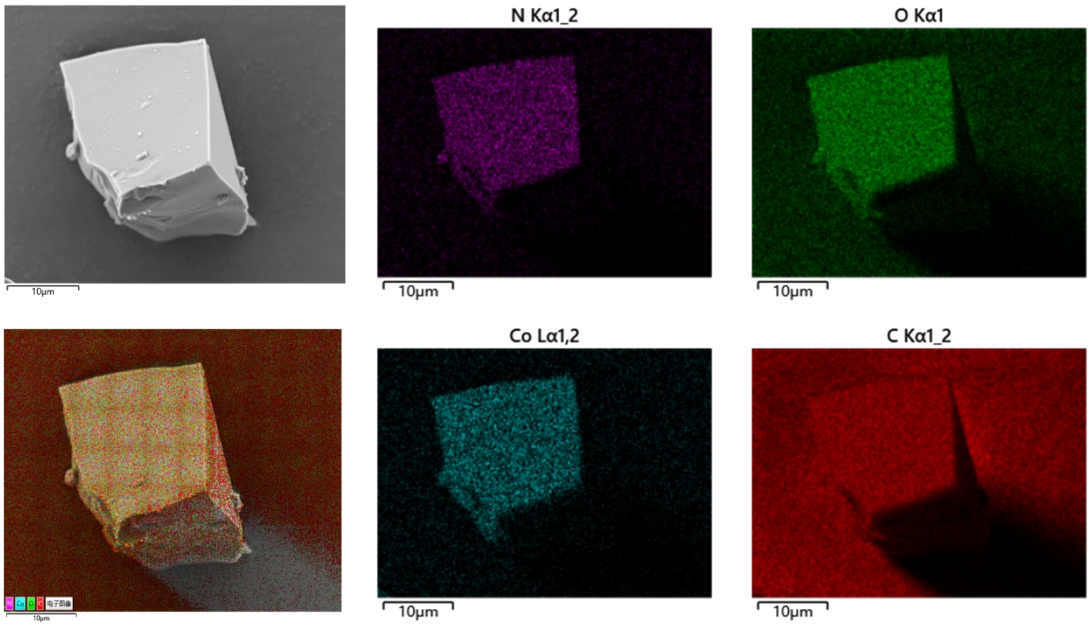

Figure S6. Element maps for Co−**CDDA**, with N (purple), O (green), Co (cyan) and C (red), manifesting that each element in Co−**CDDA** was uniformly dispersed throughout the entire structure.

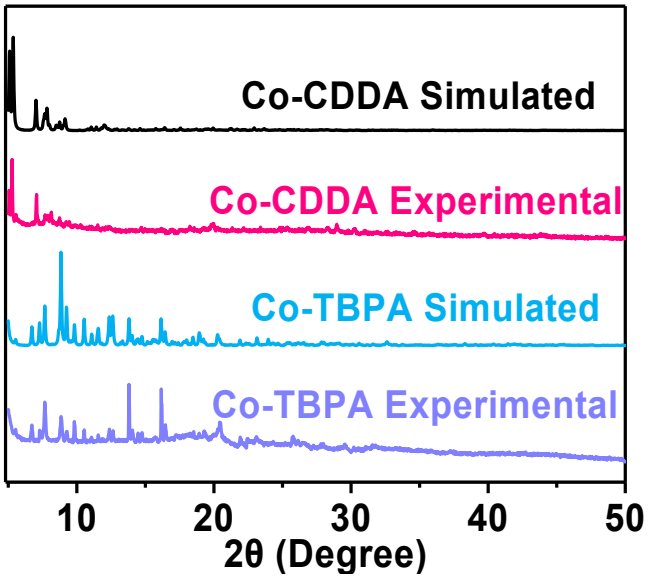

Figure S7. Powder XRD patterns of Co−**CDDA** and Co−**TBPA**, the calculated pattern based on the single-crystal simulation and as-synthesized.

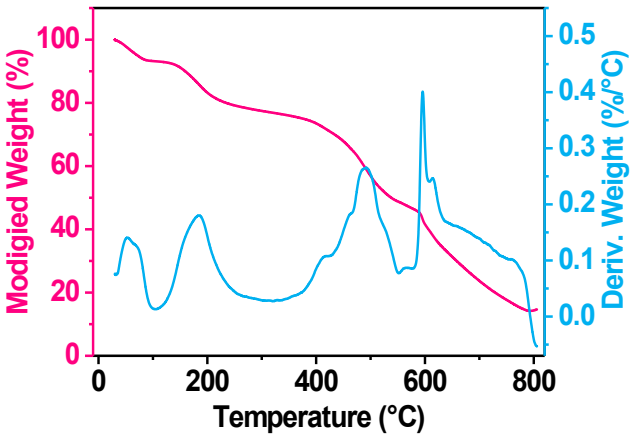

Figure S8. Thermogravimetric (TGA) analysis curve of the prepared Co−**CDDA** was carried out at a ramp rate of 10 °C min^{-1} in nitrogen flow.

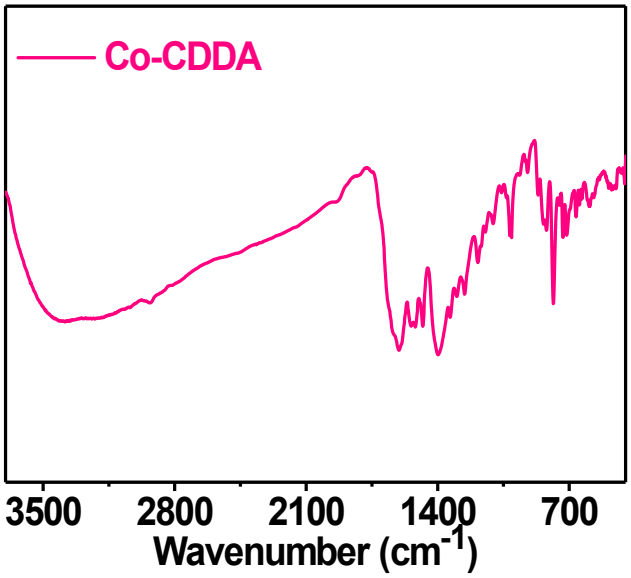

Figure S9. IR spectra of Co–**CDDA**.

Dye uptake Experiment

Firstly, Co−**MOF** (10 mg) was soaked in methanol solution (48 h) for small molecules exchange before the adsorption of dye, and then fully dried out the small molecules in a vacuum oven (60 °C, 10 h). Then, the crystals of Co−**MOF** were soaked in methanol solution of malachite green (30 mM, 2 mL), and put the vessels on a constant temperature oscillation incubator for 24 h. Then, the resulting crystals were filtered and washed with fresh methanol rapidly till the solution become colorless to thoroughly remove all the dye attached to the surface of the crystal, and then dried under ambient temperature. Then, the samples were destroyed by HCl, the resultant clear solution was diluted to 10 mL and the pH of the solution was adjusted to 1.5. The UV-vis spectrum of the above solution was performed on a UV-vis spectrophotometer. The resulting dye adsorption amount was determined by comparing the UV-vis absorption with a standard curve. The amount of malachite green uptaken by Co−**CDDA** was calculated to be 16.1% (wt%) of the framework weight and Co−**TBPA** was calculated to be 11.7% (wt%).

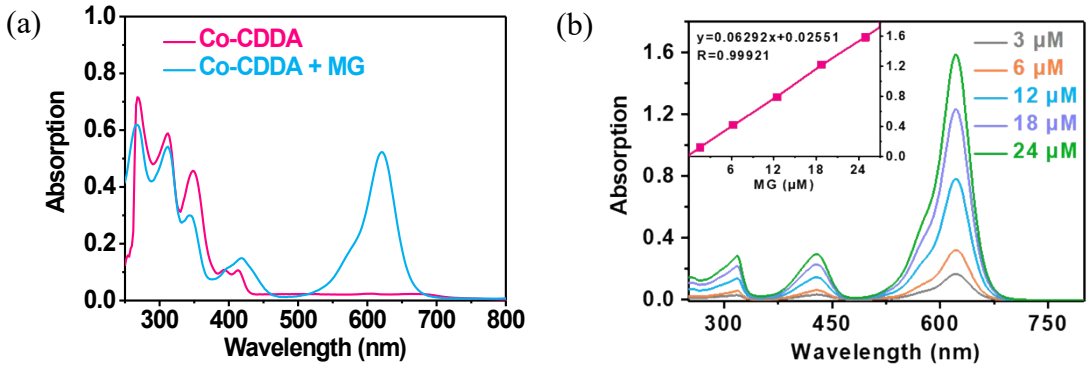

Figure S10. (a) UV-vis measurement of malachite green dye released from Co−**CDDA**. (b) UV-vis measurement of different concentrations of malachite green dye; Inside: The standard linear relationship between the absorption and the concentration of malachite green dye.

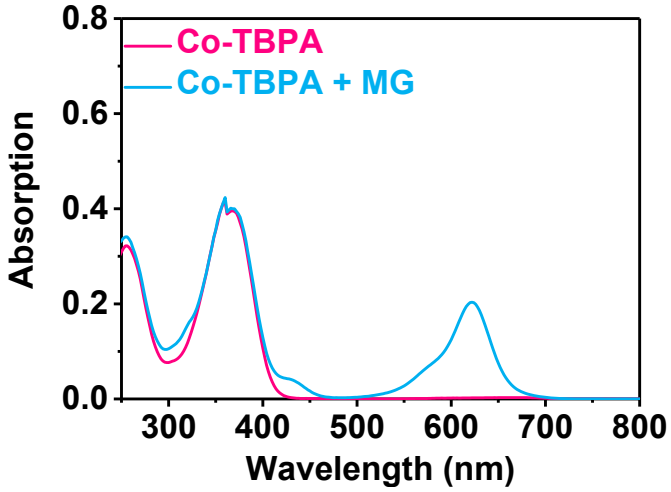

Figure S11. UV-vis measurement of malachite green dye released from Co−**TBPA**.

Confocal laser scanning microscopy

The crystals of Co−**MOF** were soaked in a methanol solution of malachite green and handled in the same way as the experiments of dye uptake mentioned above. The brightfield and confocal images of the processed samples were scanned at λ_{em} = 655−755 nm, excited by 635 nm through a 405/488/635 nm filter.

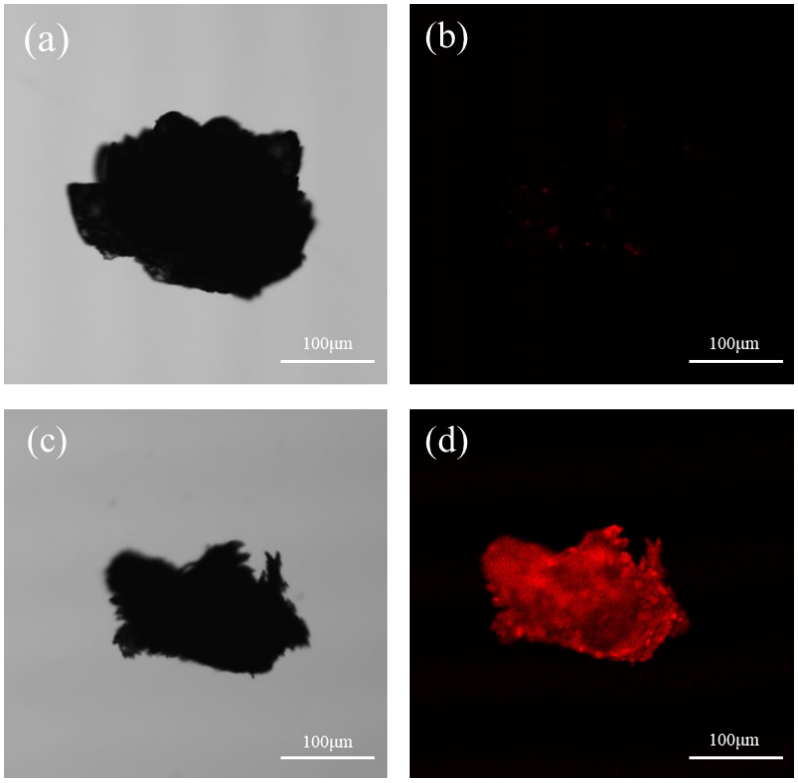

Figure S12. Laser scanning confocal microscope images of Co−**CDDA** (a and b) and malachite green dye absorbed Co−**CDDA** (c and d). Bright-field images (a and c) and dark-field images (b and d) were recorded at λ_{em} = 655−755 nm, excited by 635 nm through a 405/488/635 nm filter.

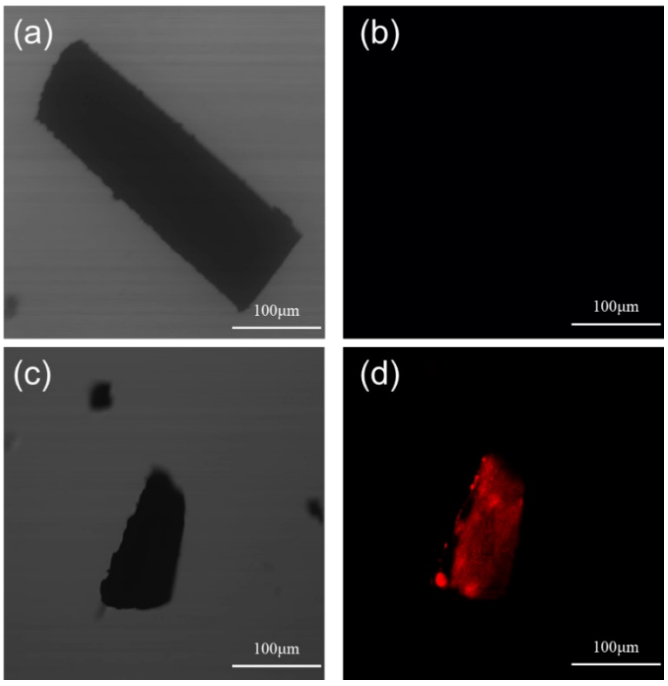

Figure S13. Laser scanning confocal microscope images of Co−**TBPA** (a and b) and malachite green dye absorbed Co−**TBPA** (c and d). Bright-field images (a and c) and dark-field images (b and d) were recorded at λ_{em} = 655−755 nm, excited by 635 nm through a 405/488/635 nm filter.

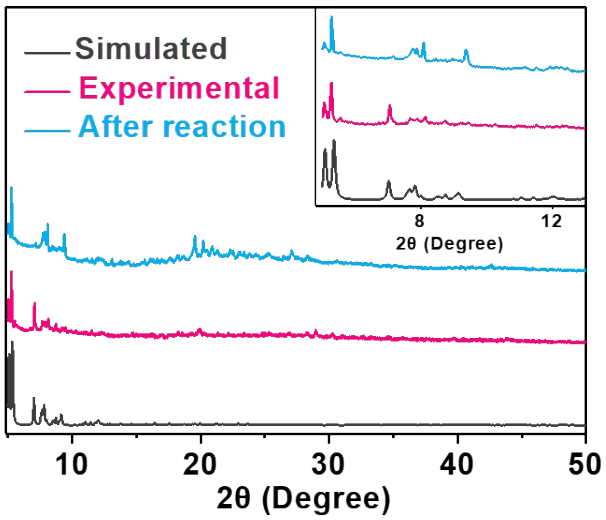

Figure S14. Powder XRD patterns of Co−**CDDA**, the calculated pattern based on the single-crystal simulation, as-synthesized and the recovery Co−**CDDA** after the catalytic process.

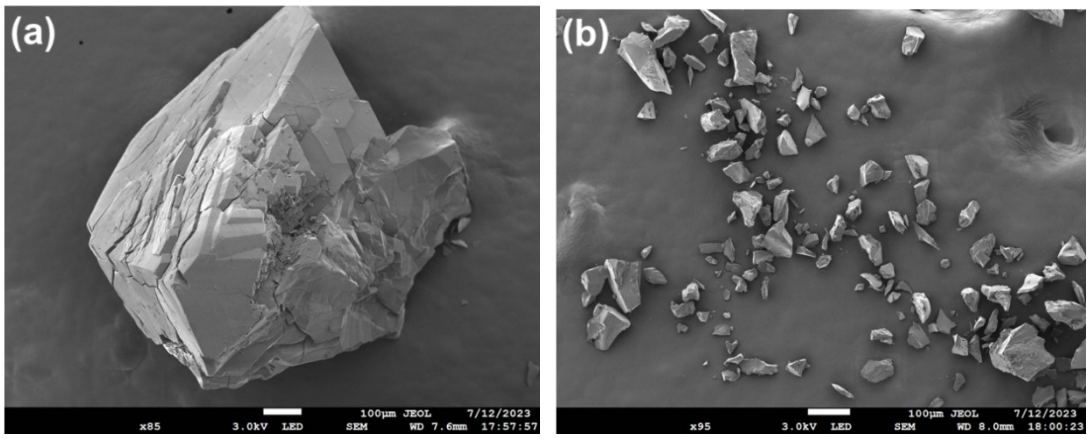

Figure S15. SEM images of Co−**CDDA** before (a) and after the catalysis (b).

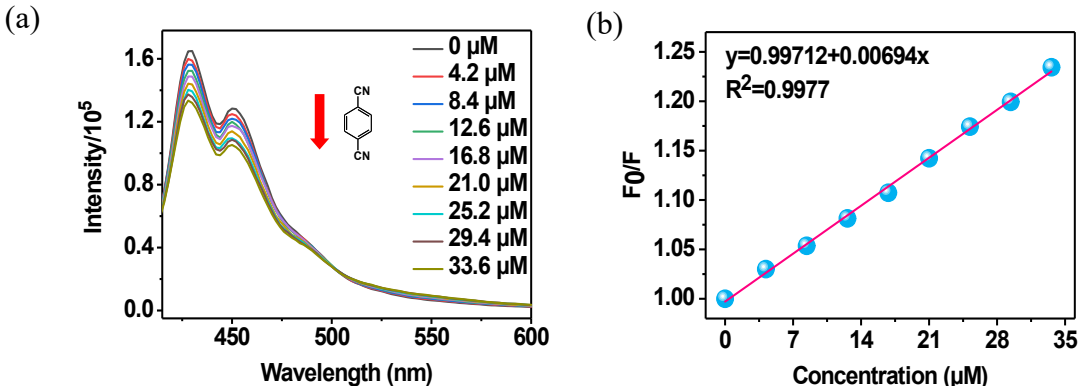

Figure S16. (a) Fluorescence titration spectra of Co−**CDDA** in DMAc suspension upon the addition of 1,4-dicyanobenzene (6.3 mM) and (b) linear relationship between the fluorescence intensity and 1,4-dicyanobenzene concentration. Fluorescence intensity was recorded at 428 nm, excited at 395 nm.

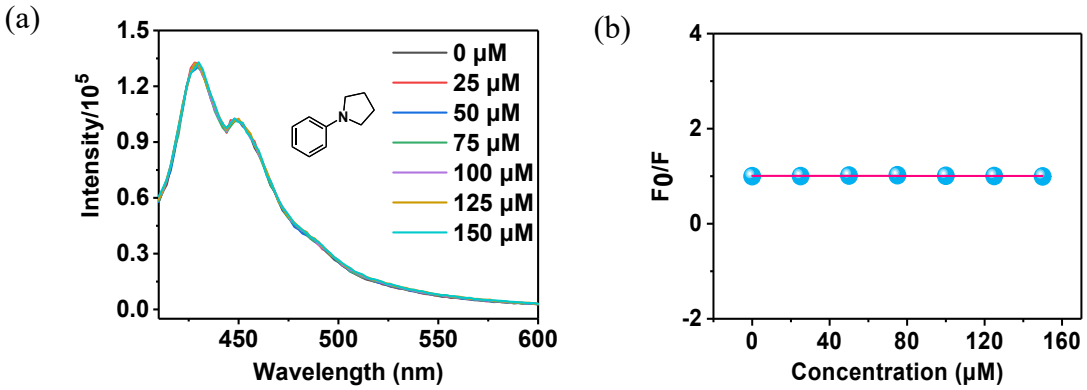

Figure S17. (a) Fluorescence titration spectra of Co−**CDDA** in DMAc suspension upon the addition of *N*-penzylpyrrolidine (25 mM) and (b) linear relationship between the fluorescence intensity and *N*-penzylpyrrolidine concentration. Fluorescence intensity was recorded at 428 nm, excited at 395 nm.

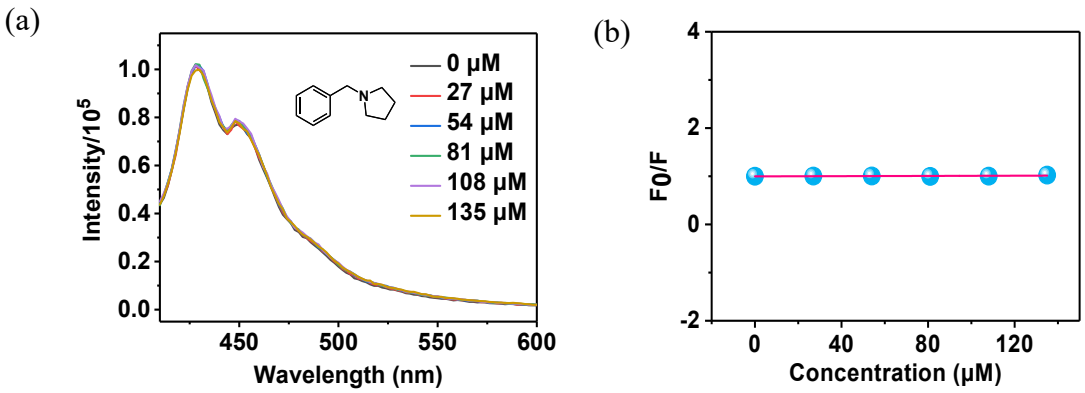

Figure S18. (a) Fluorescence titration spectra of Co−**CDDA** in DMAc suspension upon the addition of *N*-benzylpyrrolidine (18 mM) and (b) linear relationship between the fluorescence intensity and *N*-benzylpyrrolidine concentration. Fluorescence intensity was recorded at 428 nm, excited at 395 nm.

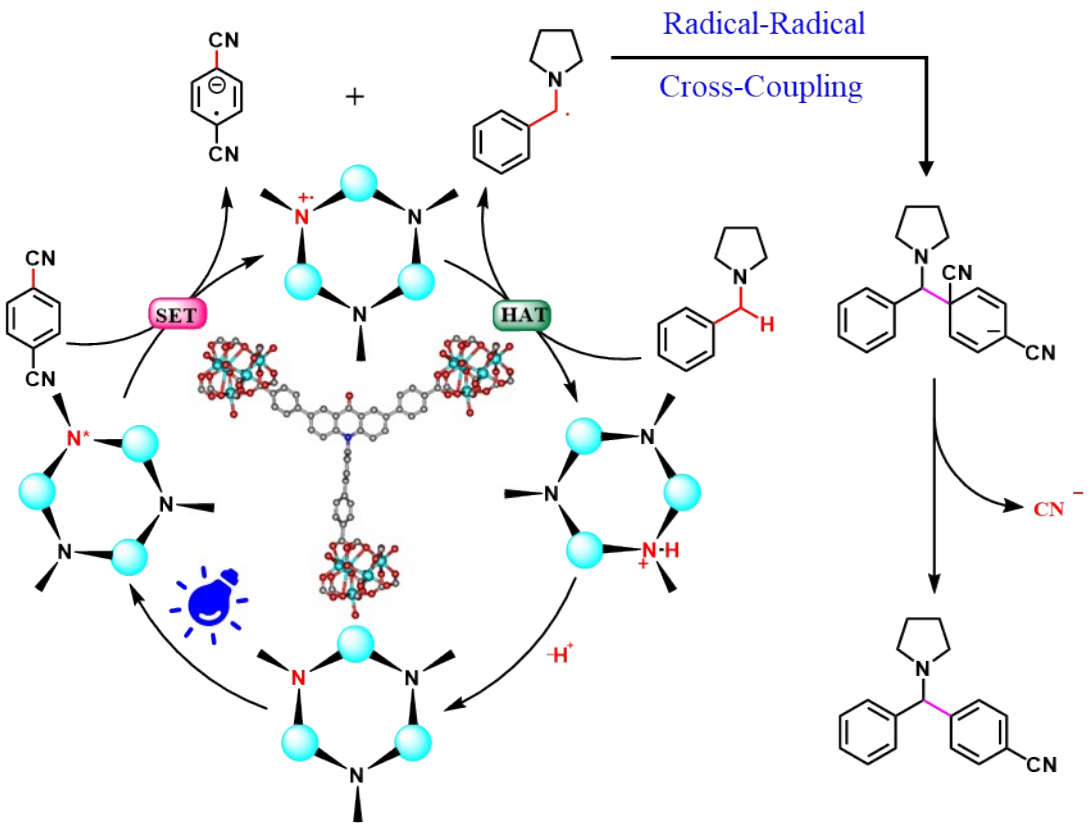

Figure S19. Proposed mechanism for regioselective C(sp^3)–H arylation reaction catalyzed by Co−**CDDA** combining the hydrogen atom transfer and photoredox catalysis.

Table S4. Photocatalytic reduction of nitrobenzene coupled with oxidation of benzylamine under different conditions[a]

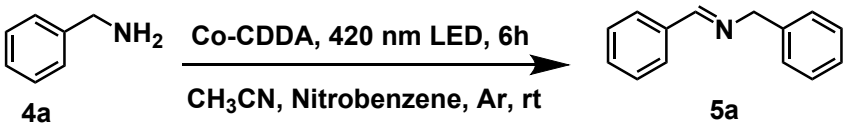

Entry	Variation from standard conditions	Yield (%)
1[b]	Co−**TBPA**	>99
2[b]	Co−**CDDA**	8.7
3	None	>99

[a] Standard conditions: Co−**CDDA** (10 μmol), nitrobenzene (0.4 mmol), benzylamine (0.2 mmol) and 4.0 mL CH_3CN for 6 h in Ar atmosphere under room temperature. Yields were determined by GC analyses using 1,3,5-Trimethoxybenzene as the internal standard. [b] Reaction conditions: 100 μL H_2O instead of nitrobenzene. Gas product was also detected by GC analyses. N.R. = No reaction.

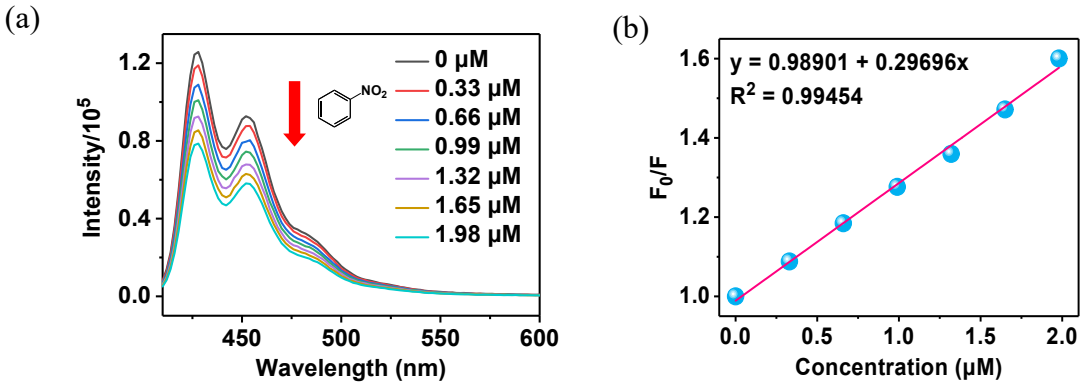

Figure 20. Fluorescence titration spectra of Co−**CDDA** in CH_3CN suspension upon the addition of nitrobenzene (0.1 mM) and (b) linear relationship between the fluorescence intensity and nitrobenzene concentration. Fluorescence intensity was recorded at 428 nm, excited at 395 nm.

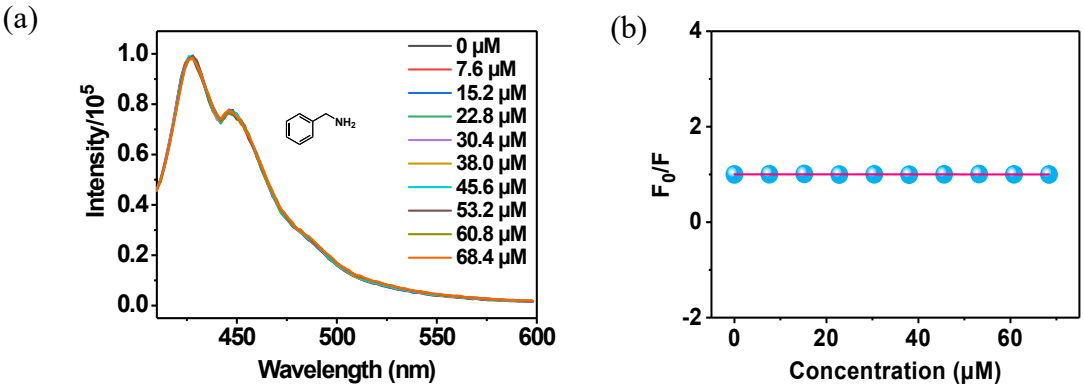

Figure S21. Fluorescence titration spectra of Co−**CDDA** in CH_3CN suspension upon the addition of benzylamine (11.4 mM) and (b) linear relationship between the fluorescence intensity and benzylamine concentration. Fluorescence intensity was recorded at 428 nm, excited at 395 nm.

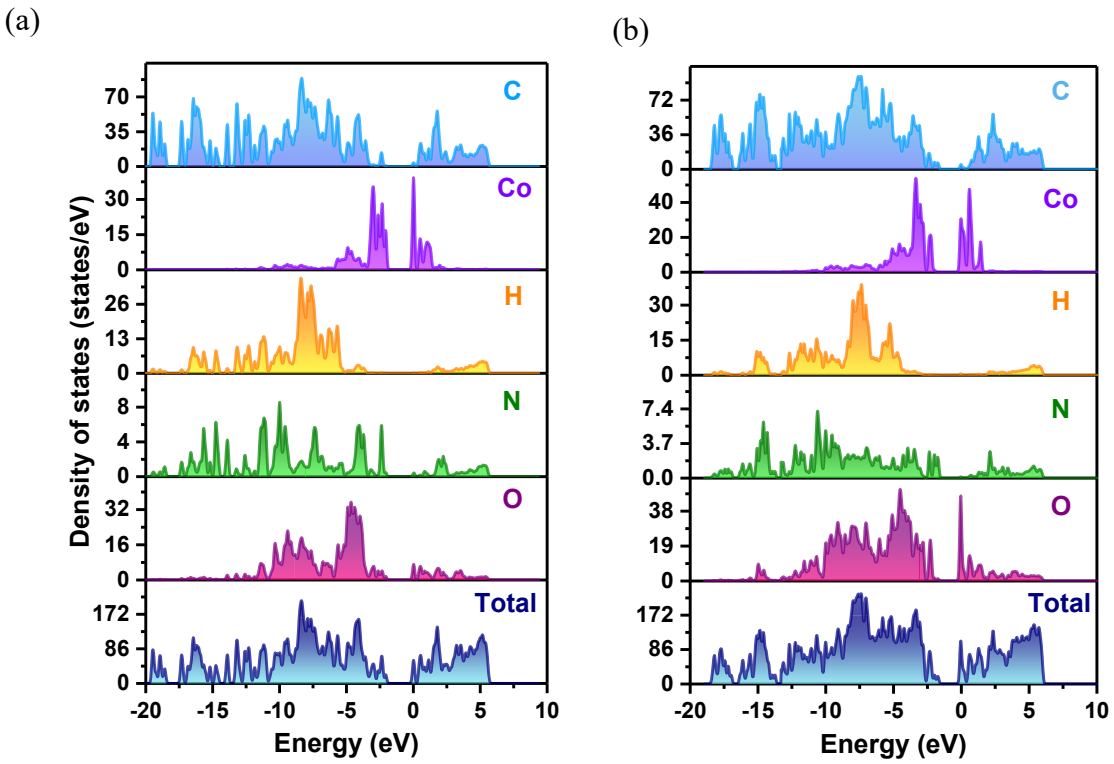

Figure S22. DOS and partials DOS plots for Co−**TBPA** (a) and Co−**CDDA** (b).

5. Catalysis Details

Deuterium labeling experiments

The deuterium labeling experiments were carried out by using *N*-((phenyl-D_5)methyl-D_2)pyrrolidine (**2k*D***) instead of *N*-benzylpyrrolidine (**2k**) as the coupling partner with 1,4-dicyanobenzene under the standard conditions. The kinetic isotope effect (KIE) was evaluated by treating *N*-benzylpyrrolidine or *N*-((phenyl-D_5)methyl-D_2)pyrrolidine in two different vessels under standard conditions, resulting in k_H/k_D as 1.72.

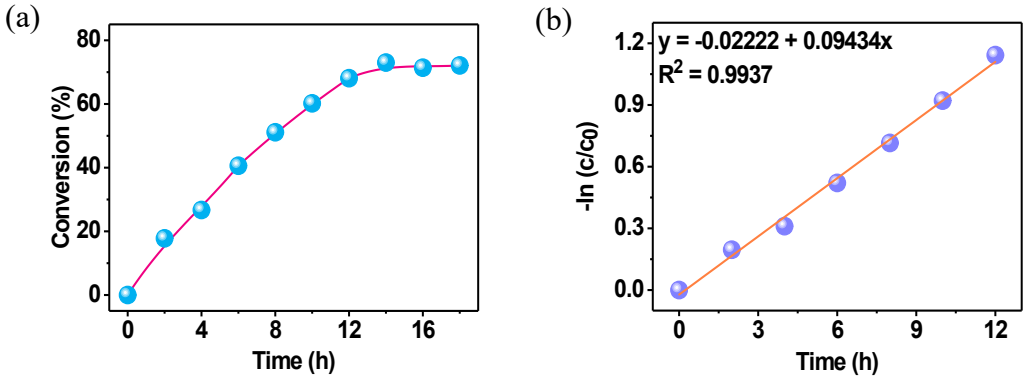

Figure S23. (a) Time-dependent catalytic rates with *N*-benzylpyrrolidine as substrate within 18 h under the standard conditions. (b) Fitting curve of the kinetic trace for the C(sp^3)–H functionalization reactions using *N*-benzylpyrrolidine as substrate.

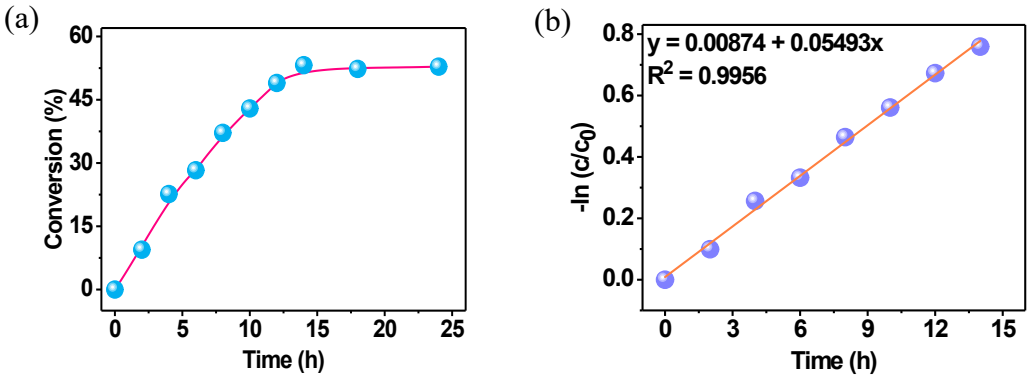

Figure S24. (a) Time-dependent catalytic rates with *N*-((phenyl-D_5)methyl-D_2)pyrrolidine as substrate within 24 h under the standard conditions. (b) Fitting curve of the kinetic trace for the C(sp^3)–H functionalization reactions using *N*-((phenyl-D_5)methyl-D_2)pyrrolidine as substrate.

General procedure for the photocatalytic α-amino C(sp^3)–H arylation of amines with 1,4-dicyanobenzene

A 10 mL flame-dried Schlenk quartz flask was filled with 1,4-dicyanobenzene (1.0 mmol), Co−**CDDA** (20.0 μmol), K_2CO_3 (1.0 mmol), amine (2.0 mmol), a mini-stirrer and DMAc (4.0 mL). Then the reaction mixture was degassed by bubbling argon for 20 minutes under atmospheric pressure. After that, the flask containing the reaction mixture was then irradiated by a 420 nm LED irradiation for 14 hours with fan cooling to maintain the flask at room temperature. After the reaction, the mixture was centrifuged at 9000 rpm for 5 min, and the supernatant was concentrated under vacuum distillation. The residues were separated on a silica gel column (EtOAc/*n*-hexane) to obtain the isolated yields.

General procedure for photocatalytic with benzylamine oxidation

A 10 mL flame-dried Schlenk quartz flask was filled with benzylamine (0.2 mmol), nitrobenzene (0.4 mmol), Co−**CDDA** (10.0 μmol), a mini-stirrer and CH_3CN (4.0 mL). Then the reaction mixture was degassed by bubbling argon for 20 minutes under atmospheric pressure. After that, the flask containing the reaction mixture was then irradiated by a 420 nm LED irradiation for 6 hours with fan cooling to maintain the flask at room temperature. After the reaction, the products were detected by GC analyses using 1,3,5-Trimethoxybenzene as the internal standard.

6. Supporting Information Spectra

compound 1: 10-(4-bromophenyl)acridin-9(10*H*)-one

Yellow solid, 93% yield. ^{1}H NMR (500 MHz, $CDCl_3$) δ 8.61 (d, J = 8.0 Hz, 2H), 7.88 (d, J = 8.2 Hz, 2H), 7.55 (t, J = 7.8 Hz, 2H), 7.36 – 7.26 (m, 4H), 6.78 (d, J = 8.6 Hz, 2H). ^{1}H NMR data matched the previously reported spectrum.[S9]

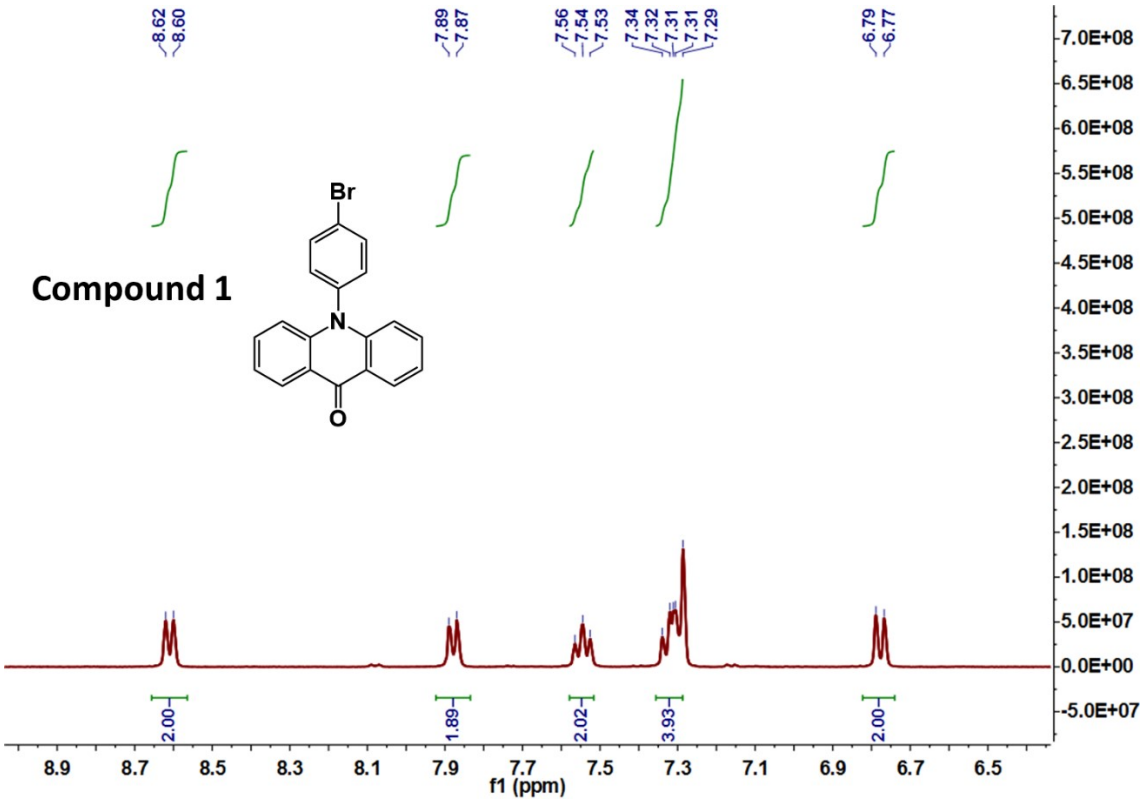

compound 2: 2,7-dibromo-10-(4-bromophenyl)acridin-9(10*H*)-one

Yellow solid, 89% yield. ^{1}H NMR (500 MHz, $CDCl_3$) δ 8.58 (d, J = 2.4 Hz, 2H), 7.80 (d, J = 4.7 Hz, 2H), 7.51 (dd, J = 9.1, 2.4 Hz, 2H), 7.17 (d, J = 1.9 Hz, 2H), 6.57 (d, J = 9.1 Hz, 2H). ^{13}C NMR (126 MHz, $CDCl_3$) δ 175.66, 141.51, 137.23, 136.59, 134.80, 131.48, 129.89, 124.39, 123.01, 118.60, 115.69. HRMS (ESI^+): Calcd. for $[C_{19}H_{10}Br_3NO + H]^+$: m/z = 507.8365, Found: 507.8356. $[C_{19}H_{10}Br_3NO + Na]^+$: m/z = 529.8185, Found: 529.8172.

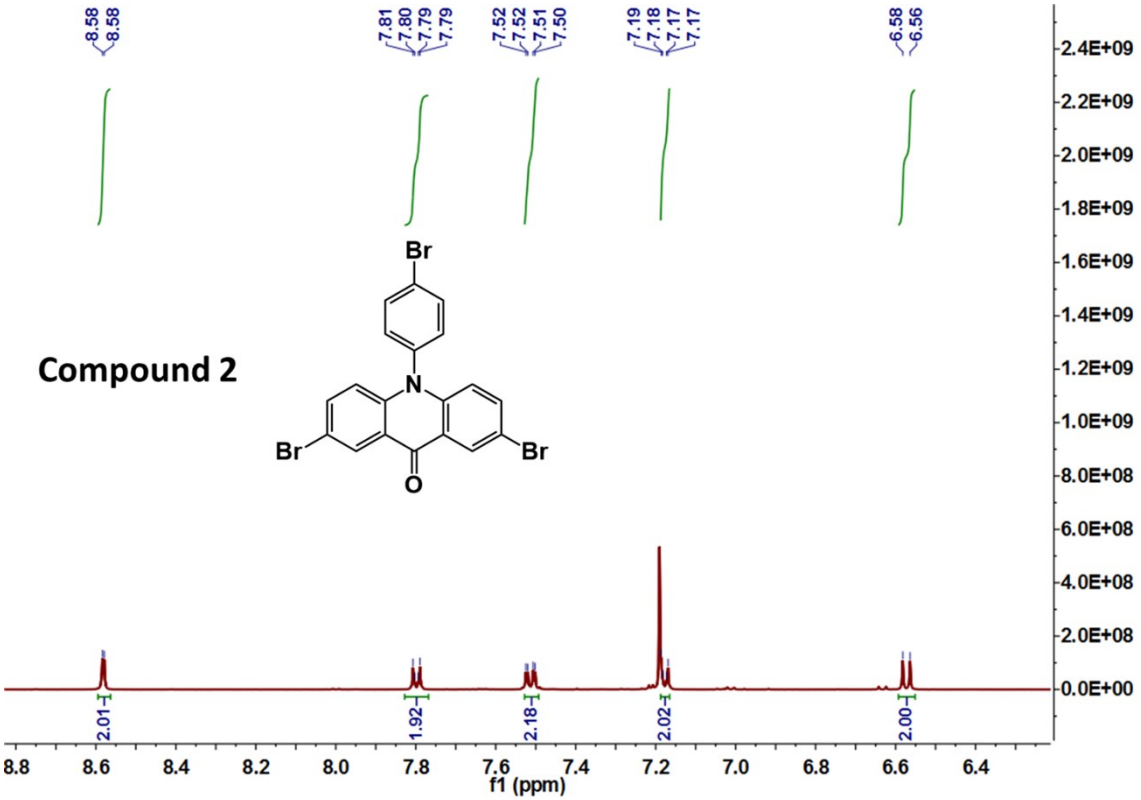

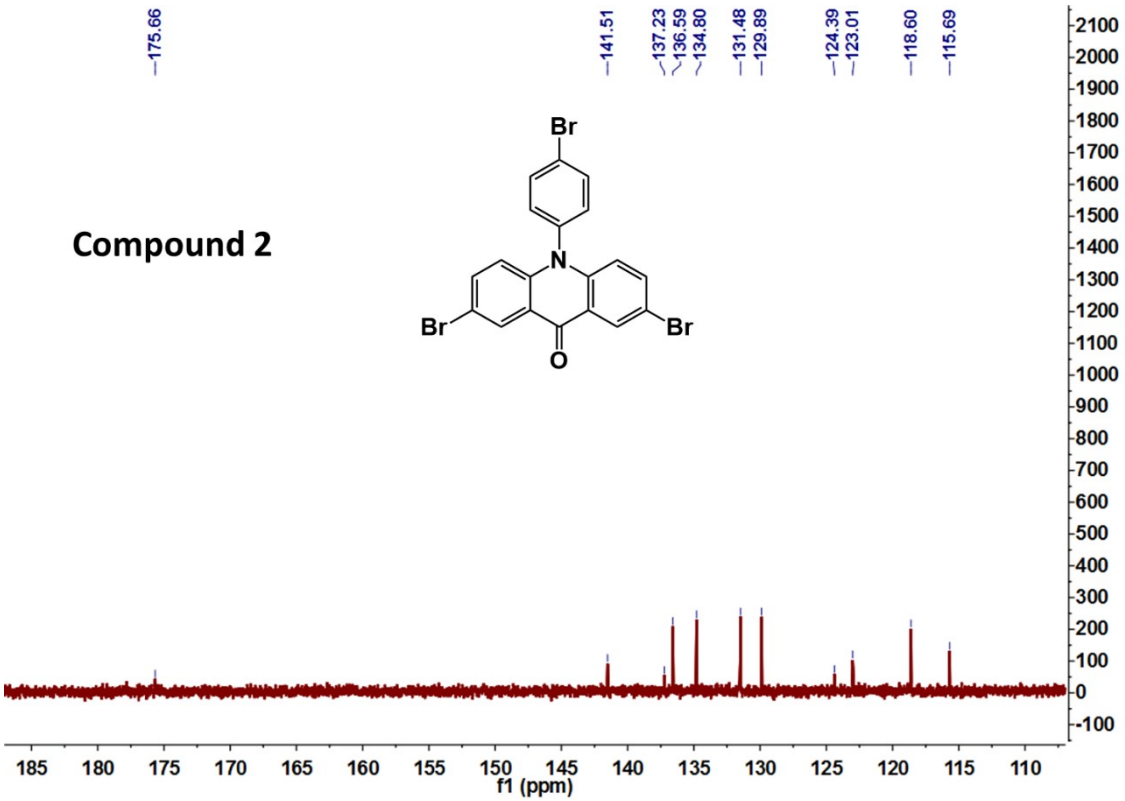
175.66
141.51
137.23
136.59
134.80
131.48
129.89
124.39
123.01
118.60
115.69
Compound 2
Br
N
Br
Br
O
f1 (ppm)

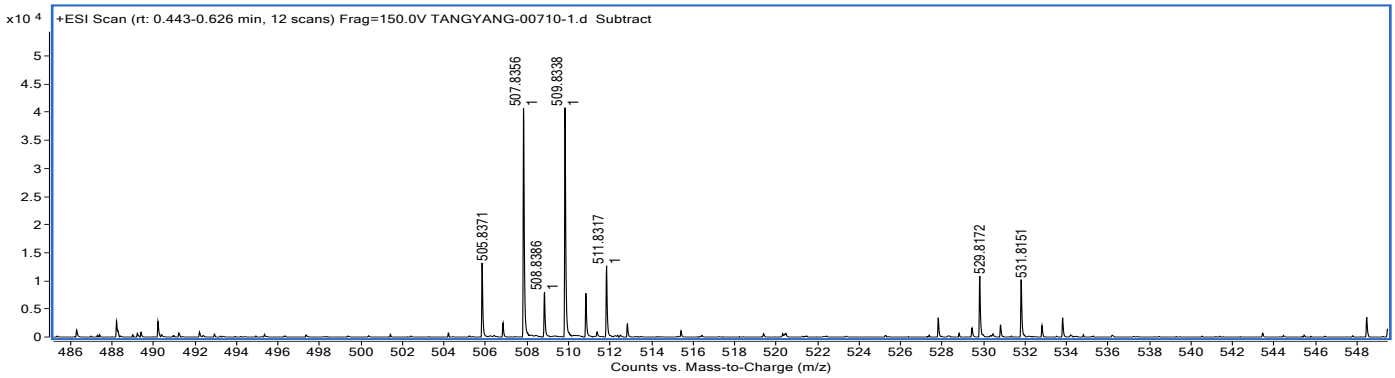
+ESI Scan (rt: 0.443-0.626 min, 12 scans) Frag=150.0V TANGYANG-00710-1.d Subtract
505.8371
507.8356
508.8386
509.8338
511.8317
529.8172
531.8151
Counts vs. Mass-to-Charge (m/z)

compound 3: 2,7-dibromo-10-(4-bromophenyl)acridin-9(10*H*)-one

Yellow solid, 72% yield. ^{1}H NMR (500 MHz, $CDCl_3$): δ 8.78 (d, J = 2.2 Hz, 2H), 8.14 (d, J = 8.3 Hz, 2H), 8.04 (d, J = 8.3 Hz, 4H), 7.92 (d, J = 8.3 Hz, 2H), 7.77 – 7.71 (m, 4H), 7.67 (t, J = 7.1 Hz, 2H), 7.46 (d, J = 8.3 Hz, 1H), 6.90 – 6.86 (m, 1H), 3.91 (s, 1H), 3.86 (s, 1H). ^{13}C NMR (126 MHz, $CDCl_3$): δ 177.89, 166.88, 166.73, 143.92, 143.82, 142.69, 141.75, 138.47, 133.46, 132.18, 130.45, 130.43, 130.27, 130.05, 129.95, 129.01, 127.24, 126.74, 125.71, 122.12, 117.74, 52.27, 52.11. HRMS (ESI$^+$): Calcd. for $[C_{43}H_{31}NO_7 + H]^+$: m/z = 674.2173, Found: 674.2176. $[C_{43}H_{31}NO_7 + Na]^+$: m/z = 696.1993, Found: 696.1988.

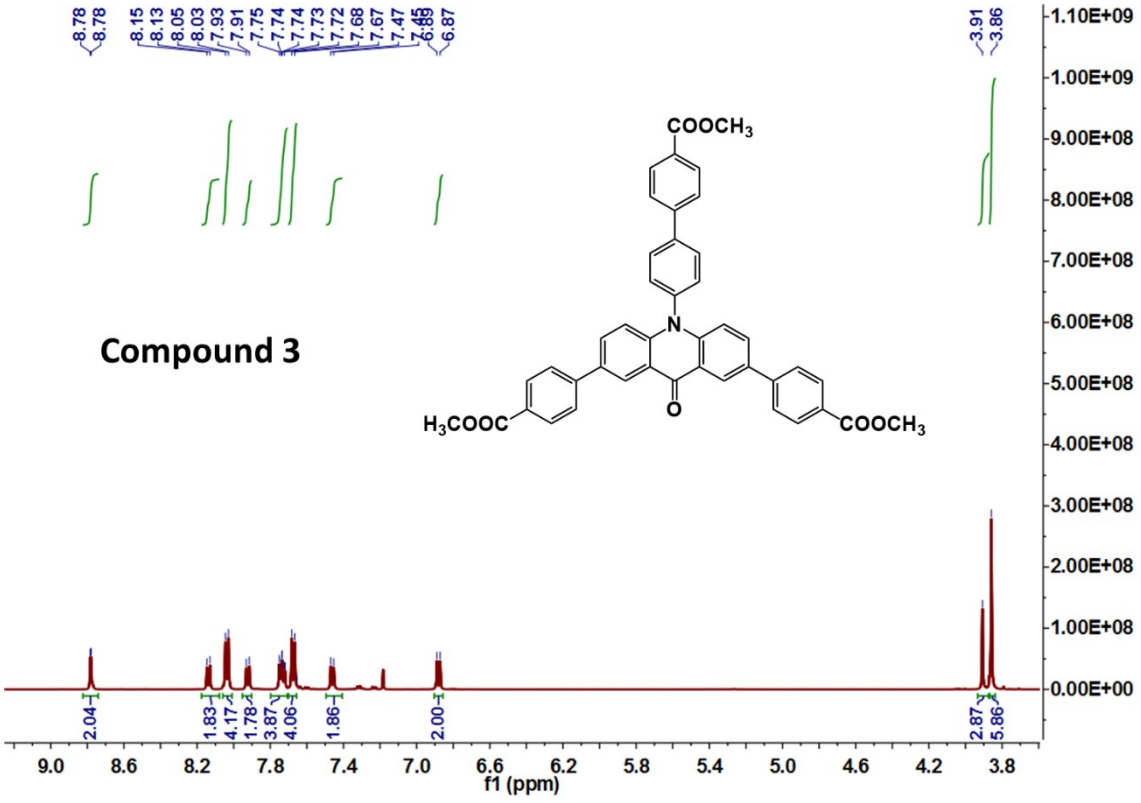

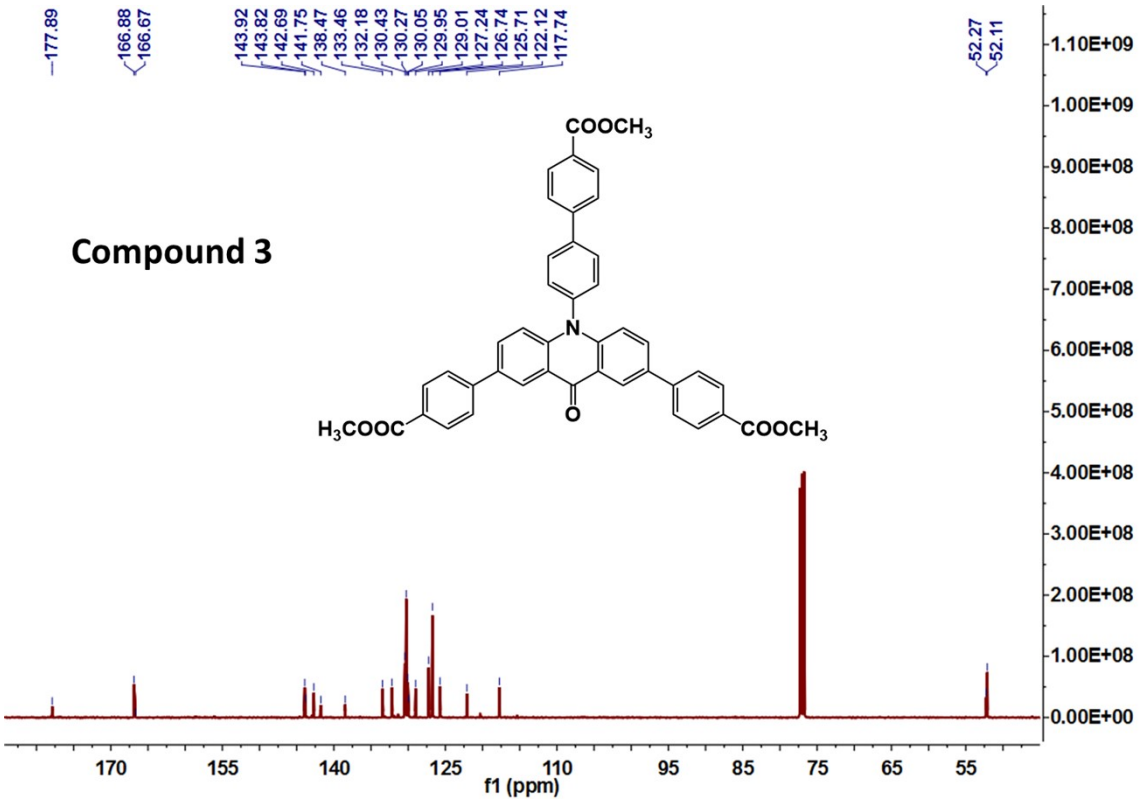
177.89
166.88
166.67
143.92
143.82
142.69
141.75
138.47
133.46
132.18
130.43
130.27
130.05
129.95
129.01
127.24
126.74
125.71
122.12
117.74
52.27
52.11
Compound 3
COOCH3
H3COOC
COOCH3
N
O
1.10E+09
1.00E+09
9.00E+08
8.00E+08
7.00E+08
6.00E+08
5.00E+08
4.00E+08
3.00E+08
2.00E+08
1.00E+08
0.00E+00
170
155
140
125
110
95
85
75
65
55
f1 (ppm)

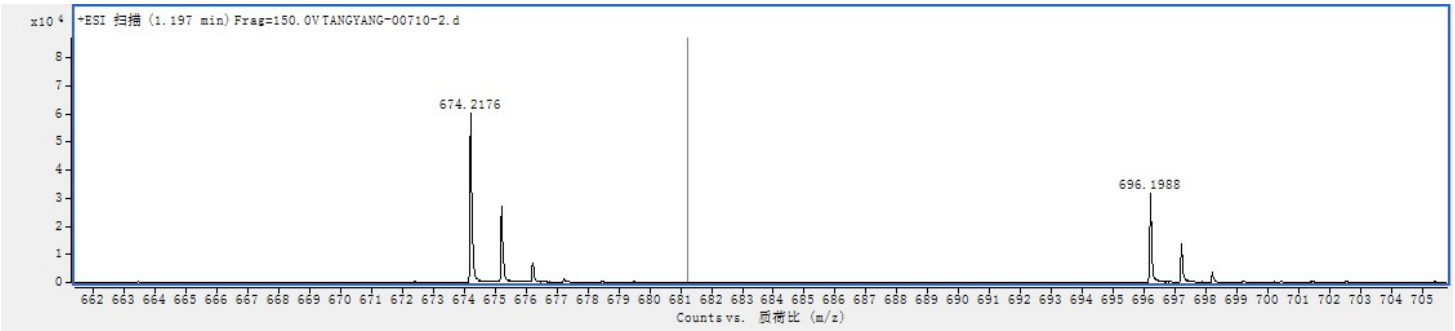
x10 4
+ESI 扫描 (1.197 min) Frag=150.0V TANGYANG-00710-2.d
674.2176
696.1988
Counts vs. 质荷比 (m/z)

H_3CDDA: 4,4'-(10-(4'-carboxy-[1,1'-biphenyl]-4-yl)-9-oxo-9,10-dihydroacridine-2,7-diyl)dibenzoic acid

Yellow solid, 90% yield. ^{1}H NMR (400 MHz, DMSO-d_6): δ 13.02 (s, 3H), 8.70 (d, J = 2.3 Hz, 2H), 8.19 (d, J = 8.4 Hz, 2H), 8.12 (d, J = 8.4 Hz, 1H), 8.09 – 8.04 (m, 3H), 8.02 (d, J = 8.4 Hz, 1H), 7.88 (d, J = 8.4 Hz, 4H), 7.77 (d, J = 8.4 Hz, 2H), 6.97 (d, J = 8.9 Hz, 2H). ^{13}C NMR (126 MHz, DMSO-d_6): δ 176.60, 167.06, 142.91, 142.86, 142.39, 140.49, 138.01, 132.45, 132.40, 130.52, 130.47, 130.33, 130.12, 130.08, 129.81, 129.63, 127.19, 126.50, 124.18, 121.36, 118.12. HRMS (ESI$^+$): Calcd. for $[C_{40}H_{24}NO_7]^-$: m/z = 630.1547, Found: 630.1554.

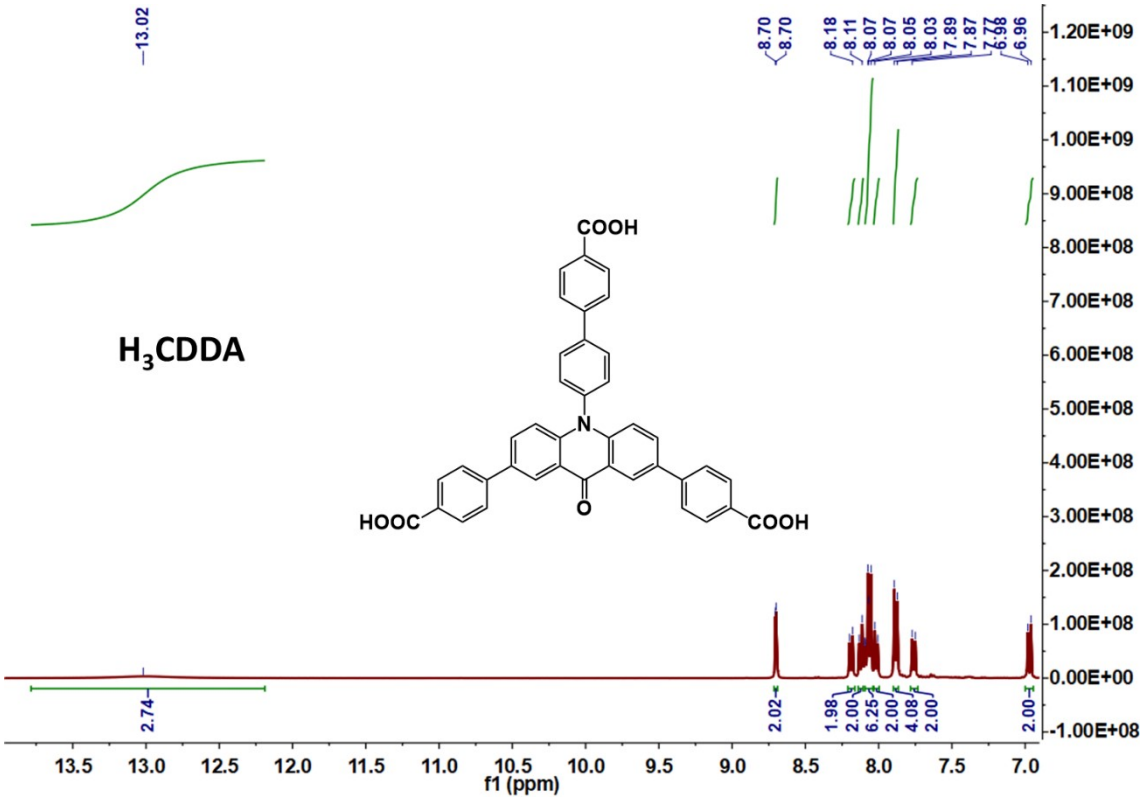

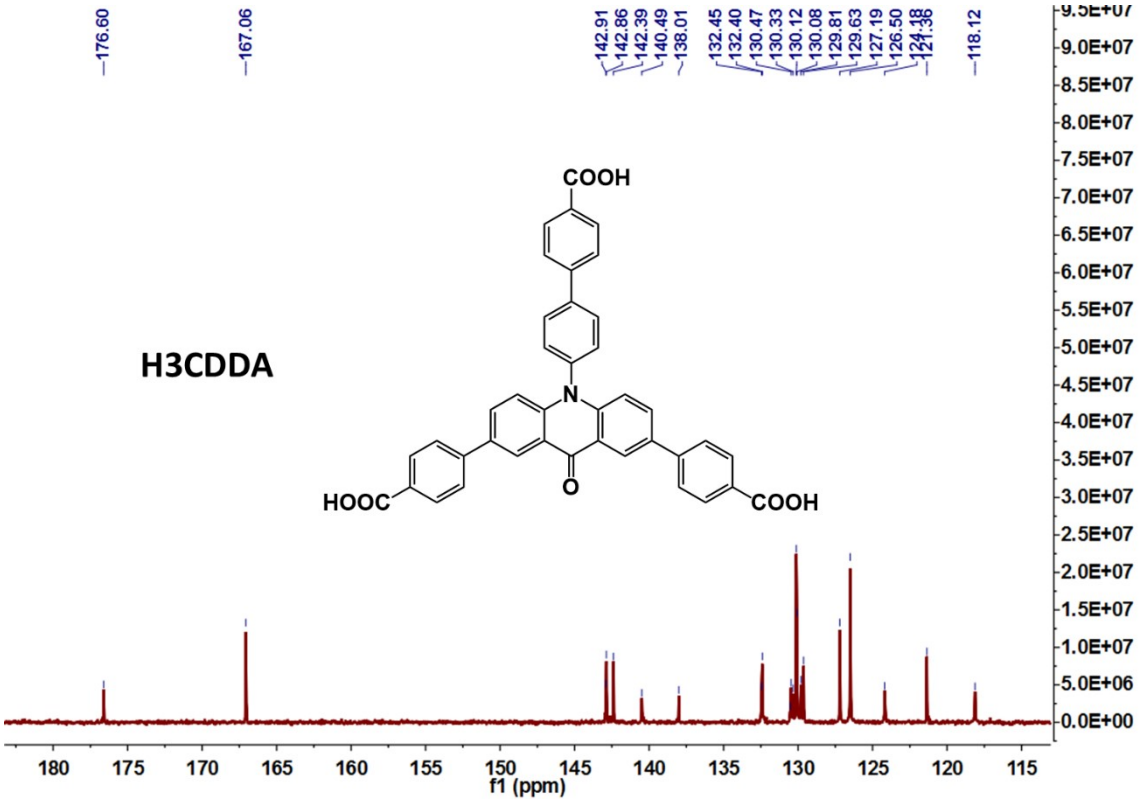
H3CDDA
COOH
HOOC
COOH
N
O
176.60
167.06
142.91
142.86
142.39
140.49
138.01
132.45
132.40
130.47
130.33
130.12
130.08
129.81
129.63
127.19
126.50
121.38
118.12
f1 (ppm)

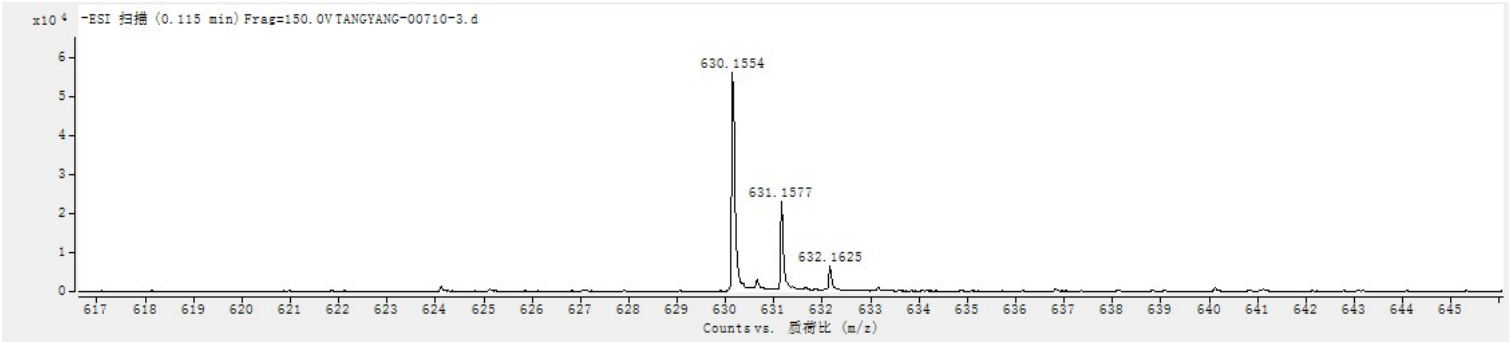
-ESI 扫描 (0.115 min) Frag=150.0V TANGYANG-00710-3.d
630.1554
631.1577
632.1625
Counts vs. 质荷比 (m/z)

3aa: 4-(1-phenylpyrrolidin-2-yl)benzonitrile

Colorless oil, 98.3% yield. ^{1}H NMR (500 MHz, $CDCl_3$) δ 7.52 (d, J = 8.3 Hz, 2H), 7.27 (d, J =8.3 Hz, 2H), 7.11 – 7.04 (m, 2H), 6.60 (t, J = 7.3 Hz, 1H), 6.36 (d, J = 8.0 Hz, 2H), 4.67 (dd, J = 8.5, 2.1 Hz, 1H), 3.72 – 3.61 (m, 1H), 3.36 (dd, J = 16.0, 8.9 Hz, 1H), 2.43 – 2.31 (m, 1H), 2.00 – 1.88 (m, 2H), 1.87 – 1.80 (m, 1H). ^{1}H NMR data matched the previously reported spectrum.[S14]

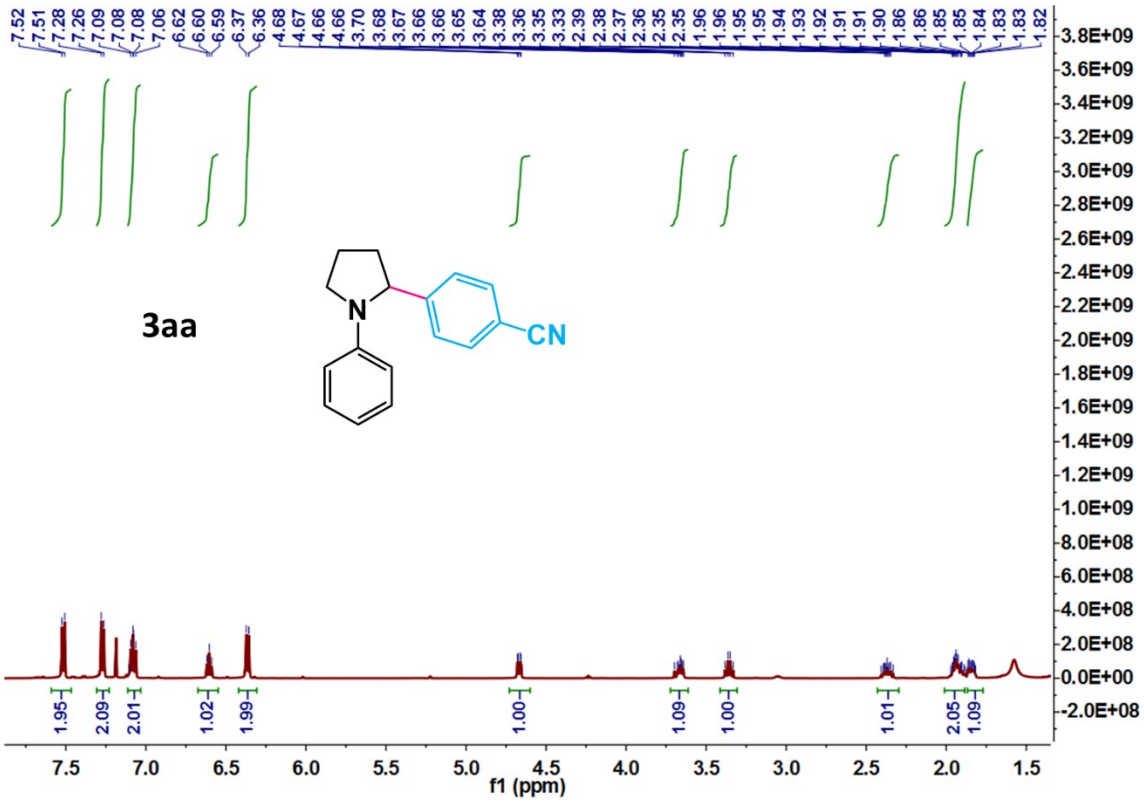

3ab: 4-(1-phenylpiperidin-2-yl)benzonitrile

Yellow oil, 78.2% yield. ^{1}H NMR (400 MHz, $CDCl_3$) δ 7.51 (d, J = 8.3 Hz, 2H), 7.40 (d, J = 8.2 Hz, 2H), 7.16 (t, J = 7.9 Hz, 2H), 6.89 (d, J = 8.0 Hz, 2H), 6.84 (t, J = 7.3 Hz, 1H), 4.42 (dd, J = 8.0, 4.0 Hz, 1H), 3.43 (dt, J = 12.1, 4.9 Hz, 1H), 3.19 – 3.09 (m, 1H), 2.05 – 1.95 (m, 1H), 1.88 – 1.68 (m, 4H), 1.63 – 1.51 (m, 1H). ^{1}H NMR data matched the previously reported spectrum.[S15]

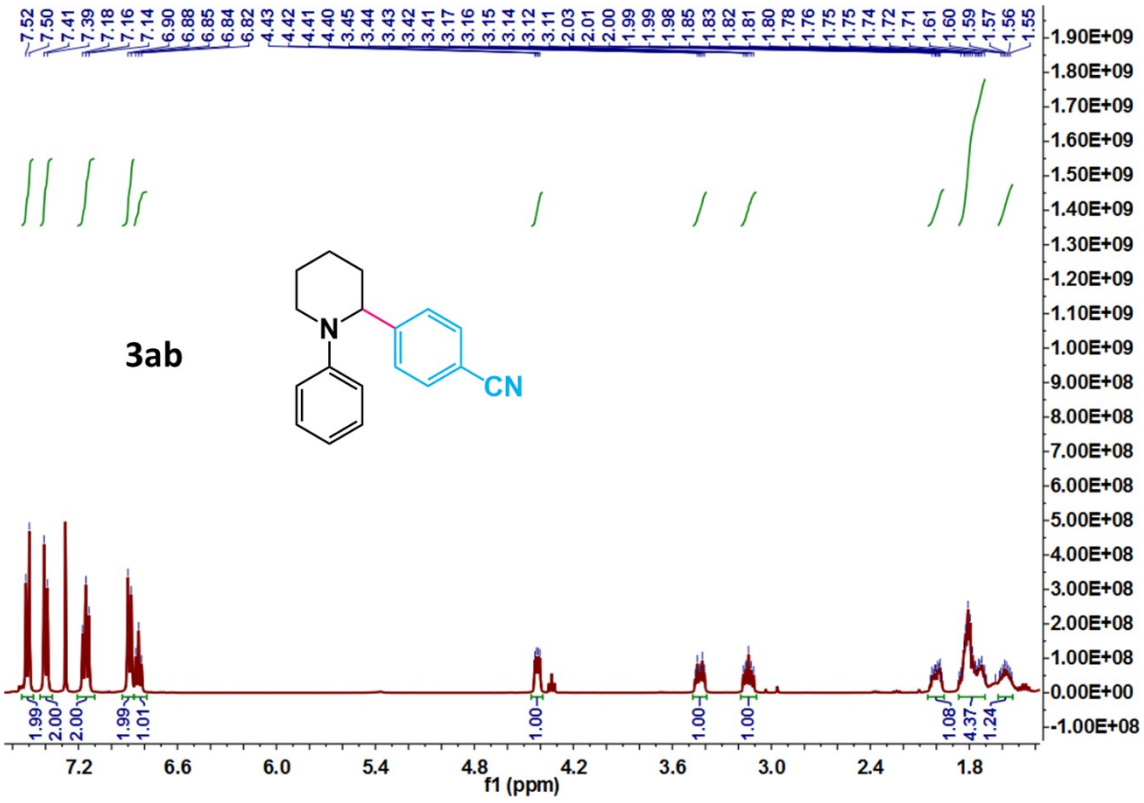

3ac: 4-(4-phenylmorpholin-3-yl)benzonitrile

Yellow oil, 70.8% yield. ^{1}H NMR (500 MHz, $CDCl_3$) δ 7.42 (d, J = 8.2 Hz, 2H), 7.36 (d, J = 8.2 Hz, 2H), 7.09 (t, J = 8.0 Hz, 2H), 6.87 – 6.76 (m, 3H), 4.35 (dd, J = 7.9, 3.5 Hz, 1H), 3.93 – 3.87 (m, 3H), 3.61 – 3.54 (m, 1H), 3.35 (dt, J = 12.4, 3.3 Hz, 1H), 3.10 – 3.03 (m, 1H). ^{1}H NMR data matched the previously reported spectrum.[S15]

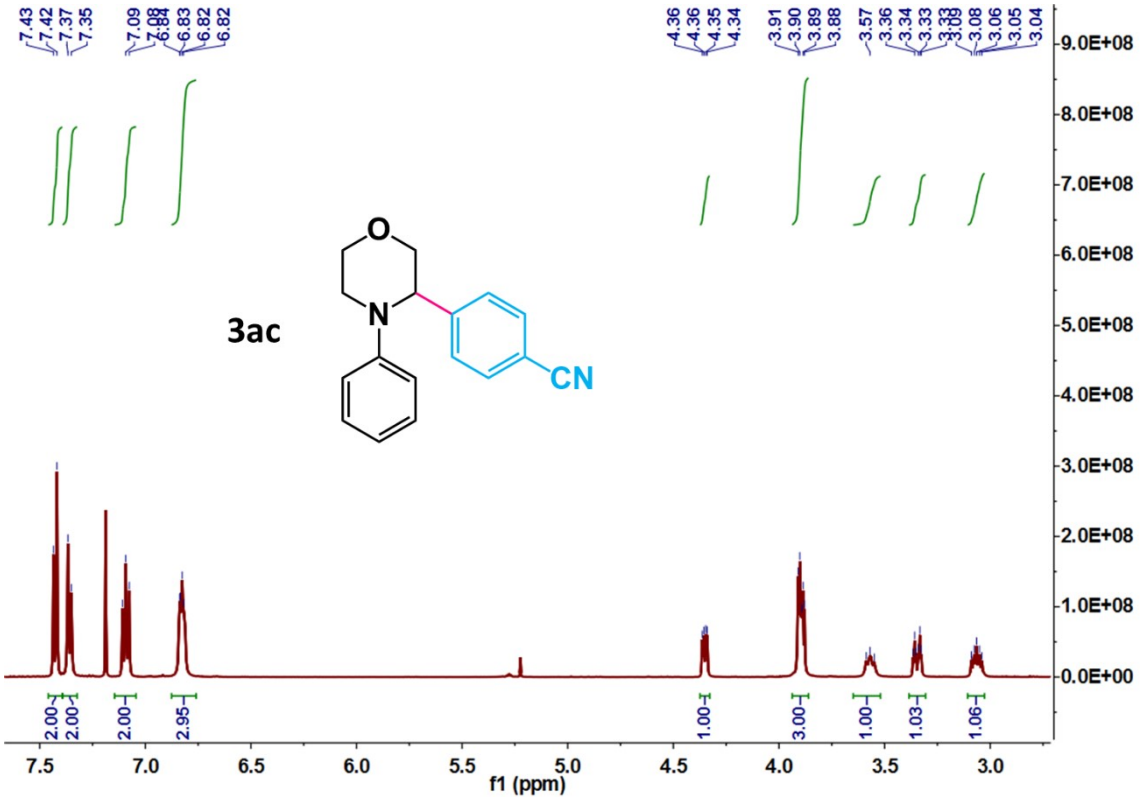

3ad: 4-((methyl(phenyl)amino)methyl)benzonitrile

Yellow oil, 94.1% yield. ^{1}H NMR (400 MHz, $CDCl_3$) δ 7.63 (d, J = 8.2 Hz, 2H), 7.37 (d, J = 8.2 Hz, 2H), 7.26 (dd, J = 8.4, 7.0 Hz, 2H), 6.78 (t, J = 7.3 Hz, 1H), 6.74 (d, J = 8.1 Hz, 2H), 4.60 (s, 2H), 3.07 (s, 3H). ^{1}H NMR data matched the previously reported spectrum.[S15]

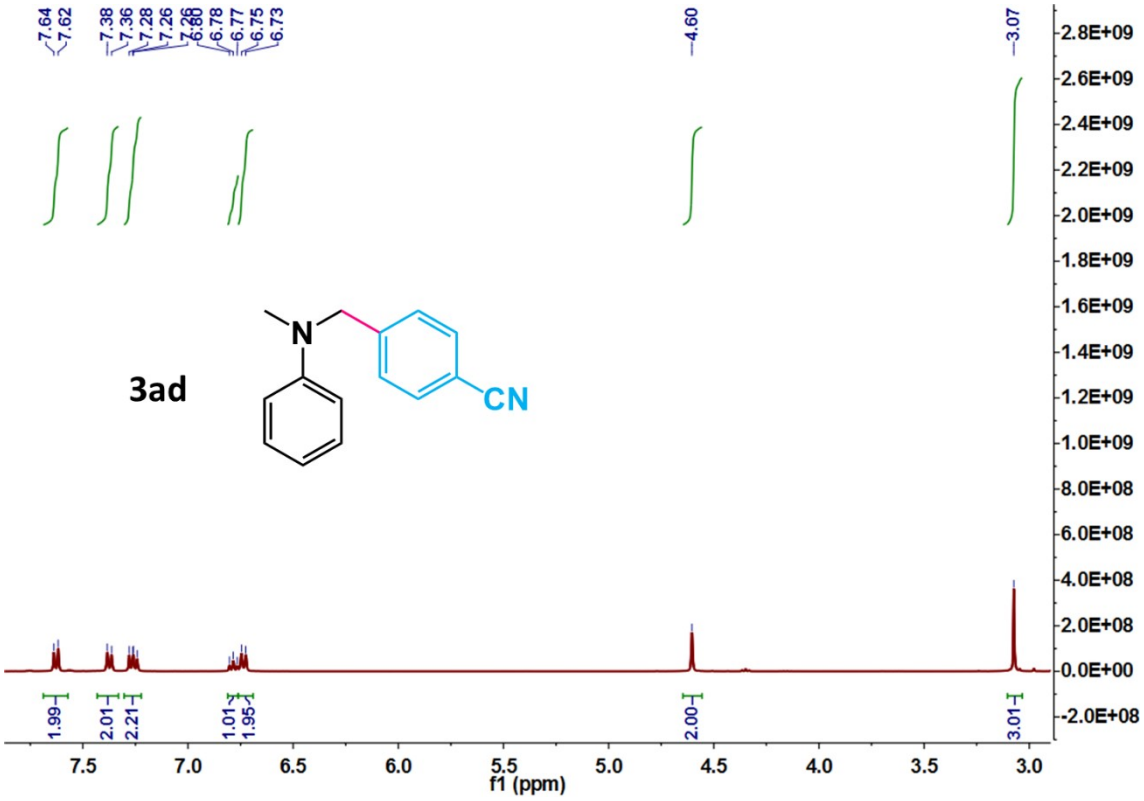

3ae: 4-(1-(ethyl(phenyl)amino)ethyl)benzonitrile

Colorless oil, 52.6% yield. ^{1}H NMR (500 MHz, $CDCl_3$) δ 7.53 (d, J = 8.4 Hz, 2H), 7.35 (d, J = 8.1 Hz, 2H), 7.15 (dd, J = 8.7, 7.3 Hz, 2H), 6.74 – 6.65 (m, 3H), 4.93 (q, J = 6.9 Hz, 1H), 3.14 (qd, J = 7.1, 2.0 Hz, 2H), 1.51 (d, J = 7.0 Hz, 3H), 1.03 (t, J = 7.0 Hz, 3H). ^{1}H NMR data matched the previously reported spectrum.[S15]

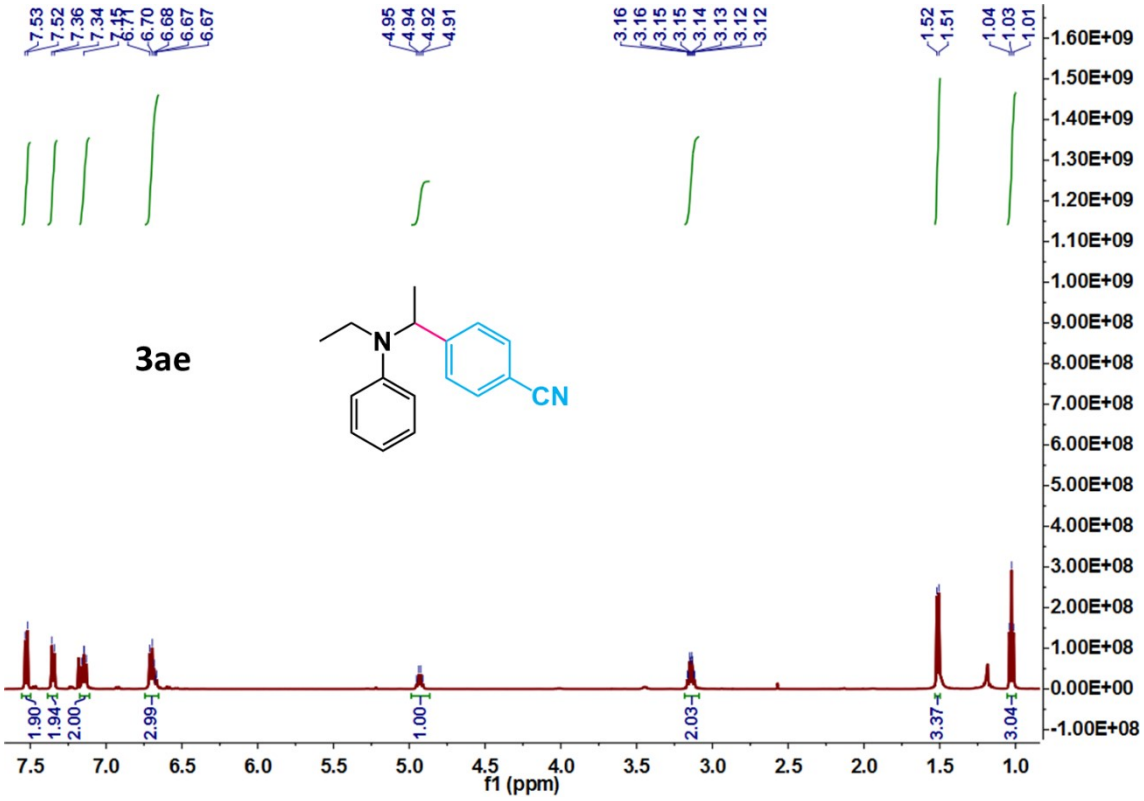

3ba: ethyl 4-(1-phenylpyrrolidin-2-yl)benzoate

Yellowish oil, 58.8% yield. ^{1}H NMR (500 MHz, $CDCl_3$) δ 7.90 (d, J = 8.3 Hz, 2H), 7.22 (d, J = 8.2 Hz, 2H), 7.06 (dd, J = 8.6, 7.4 Hz, 2H), 6.57 (t, J = 7.3 Hz, 1H), 6.39 (d, J = 7.9 Hz, 2H), 4.68 (dd, J = 8.4, 2.2 Hz, 1H), 4.29 (q, J = 7.1 Hz, 2H), 3.69 – 3.63 (m, 1H), 3.36 (q, J = 8.1 Hz, 1H), 2.40 – 2.30 (m, 1H), 1.97 – 1.91 (m, 2H), 1.89 – 1.82 (m, 1H), 1.30 (t, J = 7.1 Hz, 3H). ^{1}H NMR data matched the previously reported spectrum.[S16]

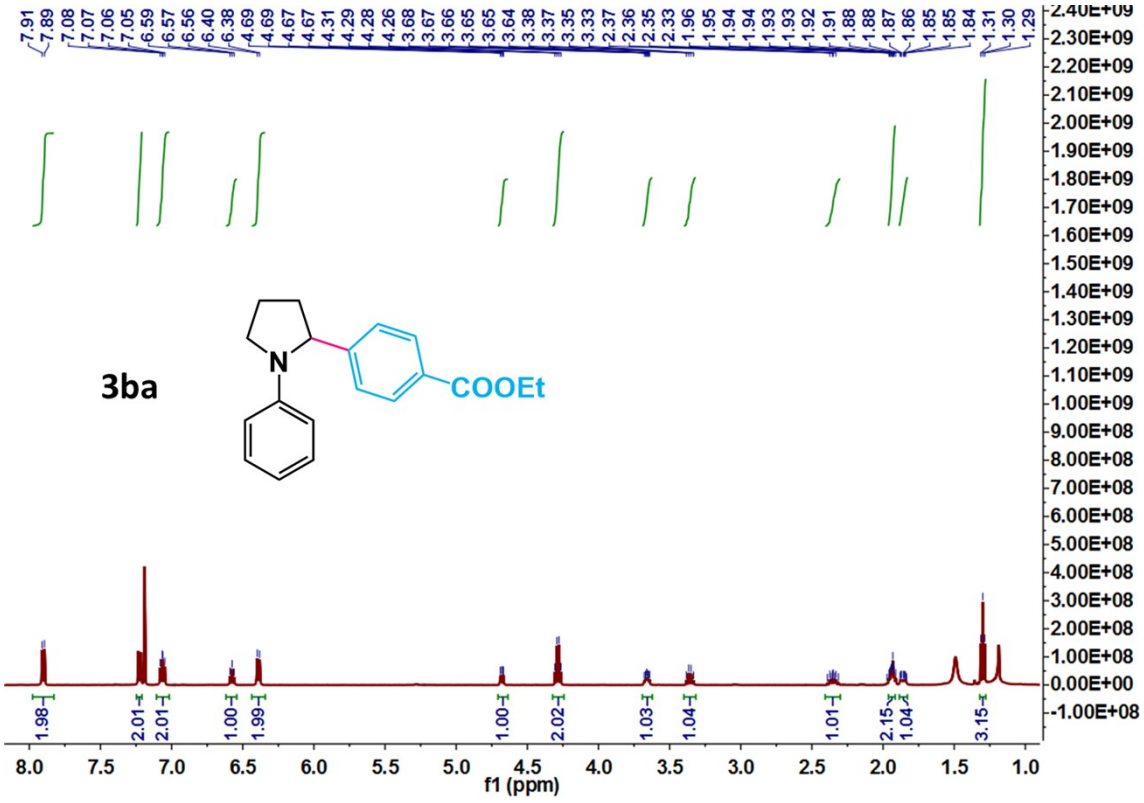

3ca: 2-(1-phenylpyrrolidin-2-yl)benzonitrile

Colorless oil, 50.7% yield. ^{1}H NMR (400 MHz, $CDCl_3$) δ7.76 – 7.65 (m, 1H), 7.53 – 7.44 (m, 1H), 7.40 – 7.25 (m, 2H), 7.22 – 7.14 (m, 2H), 6.74 – 6.67 (m, 1H), 6.48 (d, J = 8.2 Hz, 2H), 5.08 (d, J = 7.9 Hz, 1H), 3.89 – 3.67 (m, 1H), 3.57 – 3.35 (m, 1H), 2.68-2.45 (m , 1H), 2.15 – 1.93 (m, 3H). ^{1}H NMR data matched the previously reported spectrum.[S15]

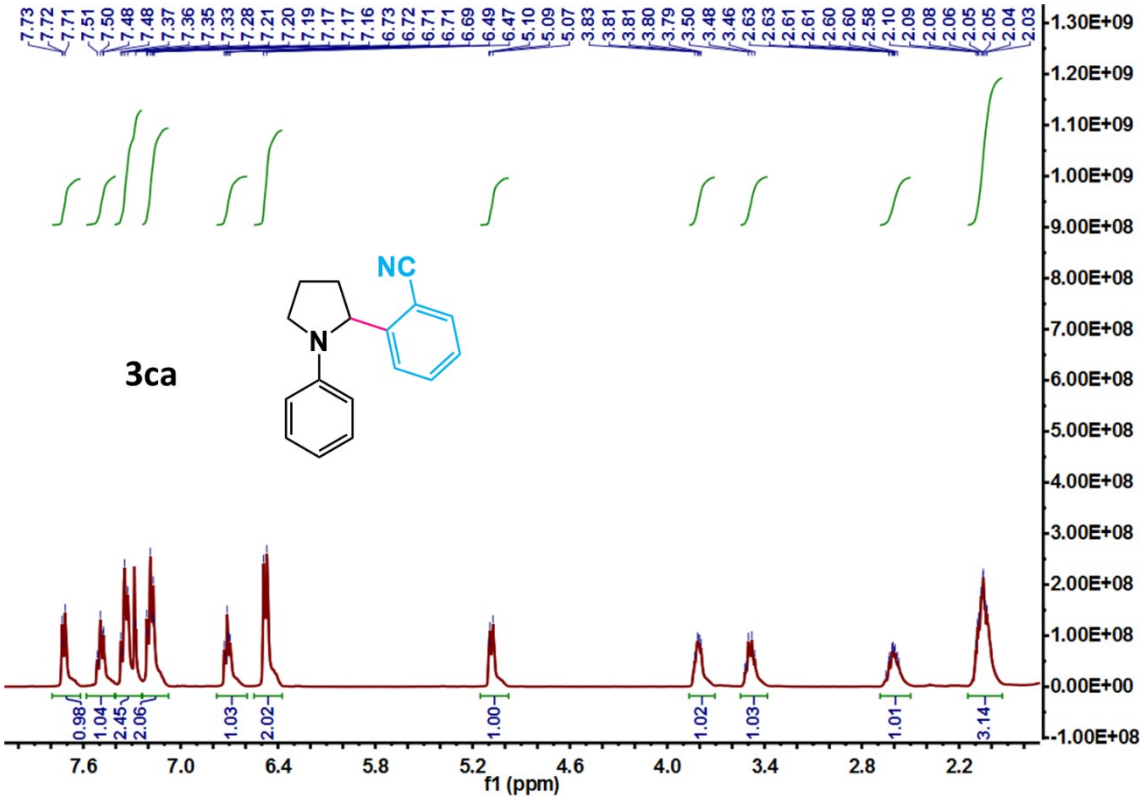

3da: 2-methyl-4-(1-phenylpyrrolidin-2-yl)pyridine

Yellow oil, 91.7% yield. ^{1}H NMR (400 MHz, $CDCl_3$) δ 8.39 (d, J = 5.1 Hz, 1H), 7.14 (t, J = 7.9 Hz, 2H), 7.02 (s, 1H), 6.96 (d, J = 5.1 Hz, 1H), 6.67 (t, J = 7.3 Hz, 1H), 6.45 (d, J = 8.1 Hz, 2H), 4.62 (d, J = 7.2 Hz, 1H), 3.82 – 3.65 (m, 1H), 3.40 (q, J = 8.3 Hz, 1H), 2.51 (s, 3H), 2.45 – 2.33 (m, 1H), 2.05-1.96 (m, 2H), 1.94-1.86 (m, 1H). ^{1}H NMR data matched the previously reported spectrum.[S16]

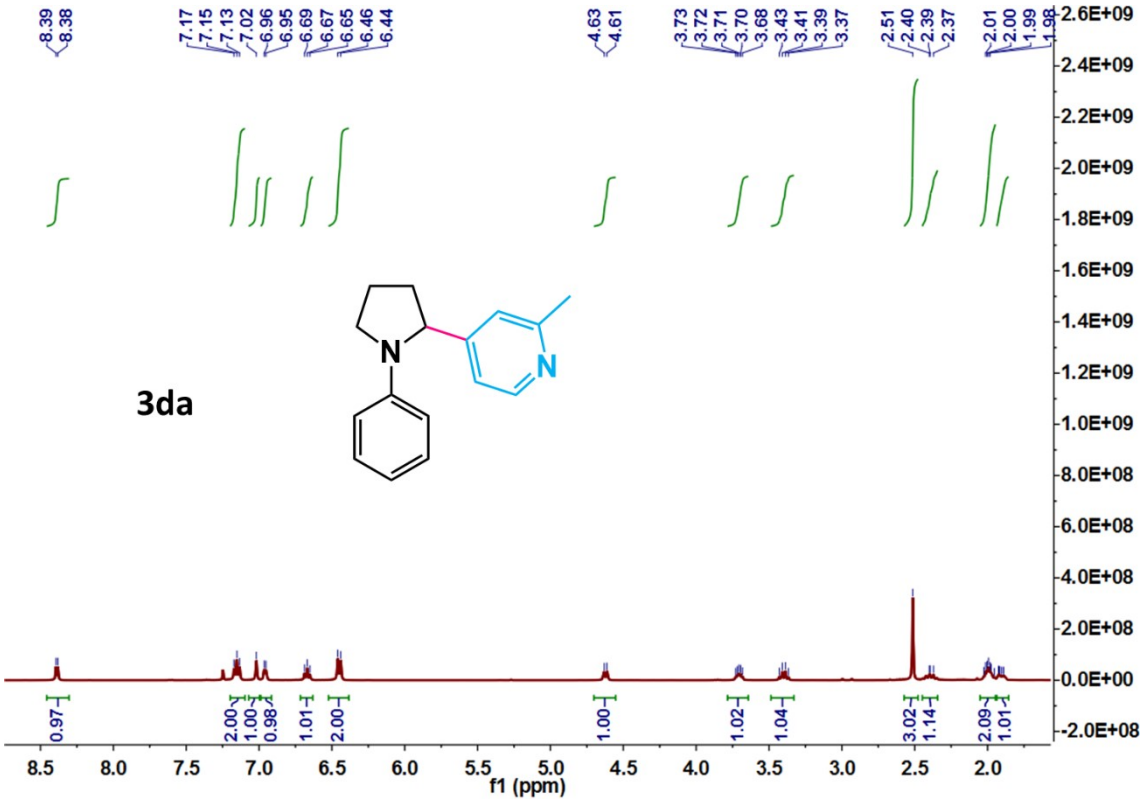

3ea: 4-(1-phenylpyrrolidin-2-yl)pyridine

Yellowish oil, 77.4% yield. ^{1}H NMR (400 MHz, $CDCl_3$) δ 8.54 (d, J = 5.1 Hz, 2H), 7.18 (t, J = 6.4 Hz, 4H), 6.70 (t, J = 7.3 Hz, 1H), 6.47 (d, J = 8.2 Hz, 2H), 4.70 (d, J = 7.8 Hz, 1H), 3.81 – 3.65 (m, 1H), 3.45 (dd, J = 16.2, 8.7 Hz, 1H), 2.52 – 2.39 (m, 1H), 2.08 – 1.99 (m, 2H), 1.98-1.89 (m, 1H). ^{1}H NMR data matched the previously reported spectrum.[S16]

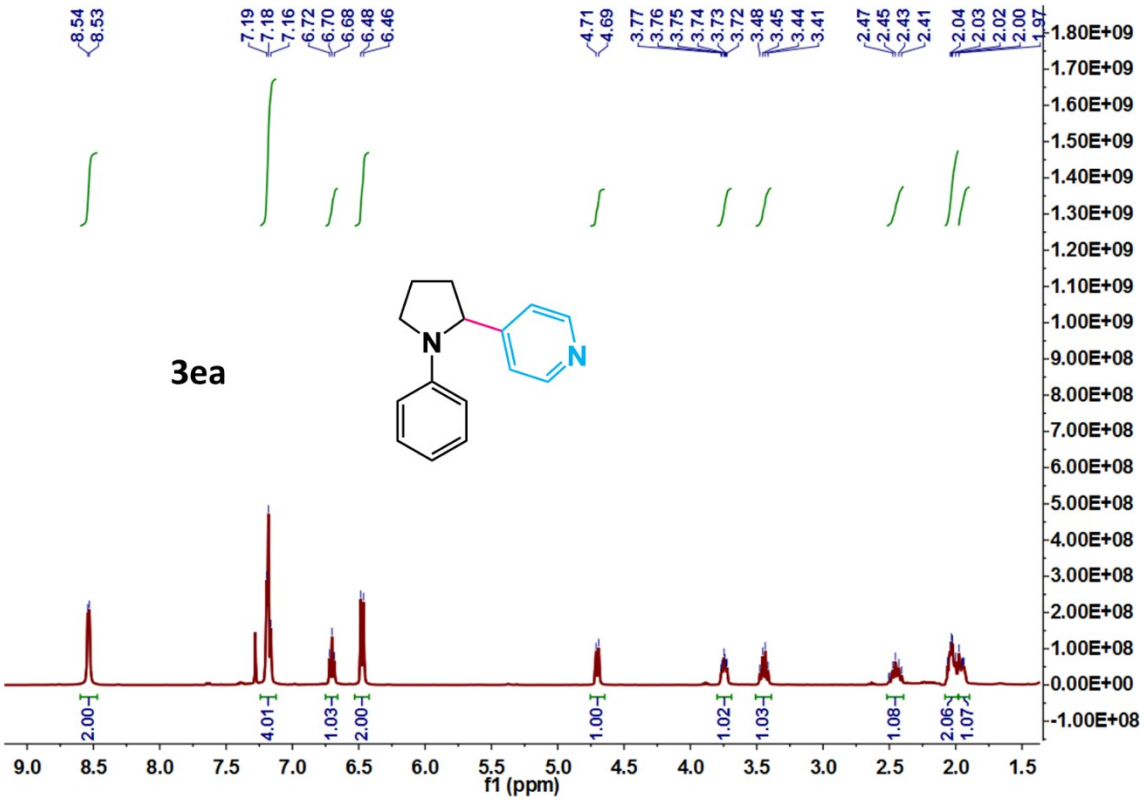

3fa: 2-(1-phenylpyrrolidin-2-yl)pyridine

Yellowish oil, 45.2% yield. ^{1}H NMR (400 MHz, $CDCl_3$) δ 8.63 (d, J = 4.7 Hz, 1H), 7.57 (td, J = 7.7, 1.7 Hz, 1H), 7.20 – 7.13 (m, 4H), 6.68 (t, J = 7.3 Hz, 1H), 6.52 (d, J = 8.2 Hz, 2H), 4.85 (dd, J = 8.6, 2.1 Hz, 1H), 3.80 – 3.71 (m, 1H), 3.46 (dd, J = 16.3, 8.9 Hz, 1H), 2.54 – 2.41 (m, 1H), 2.19-2.11 (m, 1H), 2.08 – 1.92 (m, 2H). ^{1}H NMR data matched the previously reported spectrum.[S16]

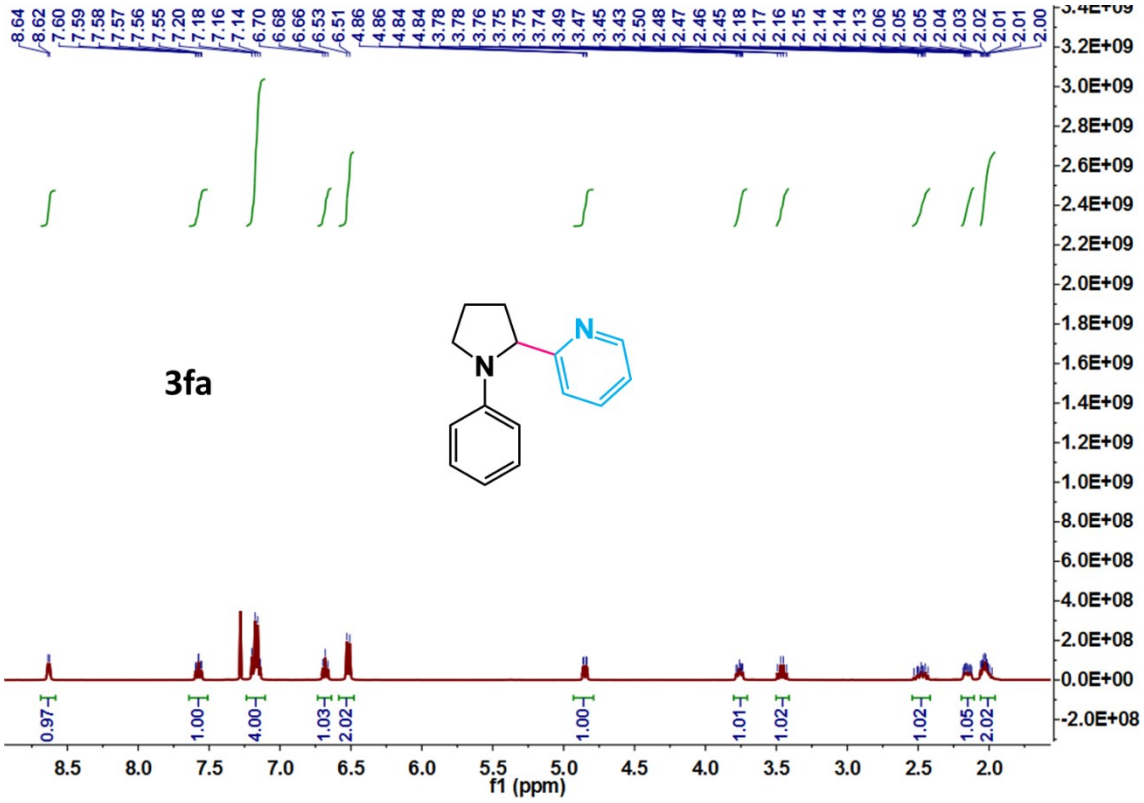

3af: 4-((diethylamino)(phenyl)methyl)benzonitrile

Colorless oil, 62.4% yield. ^{1}H NMR (400 MHz, $CDCl_3$) δ 7.58 (m, 4H), 7.40 – 7.18 (m, 5H), 4.78 (s, 1H), 2.72 – 2.37 (m, 4H), 1.00 (t, J = 7.0 Hz, 6H).^{1}H NMR data matched previously reported spectrum.[S17]

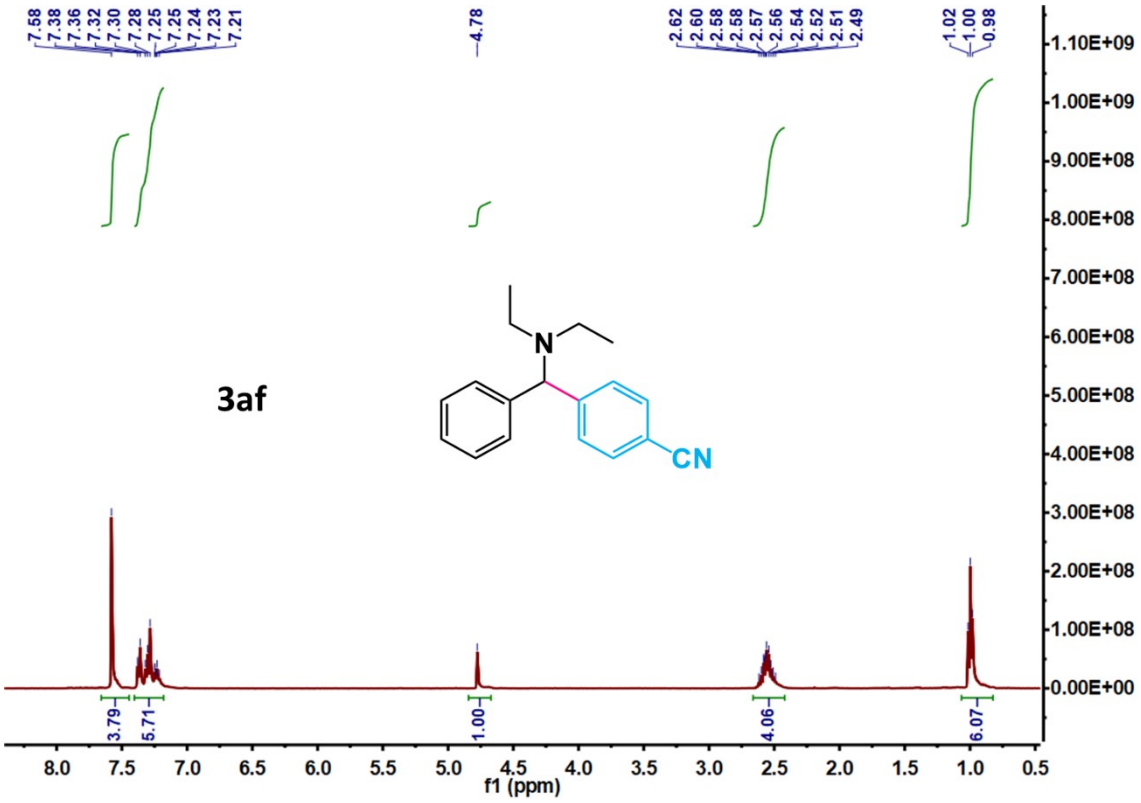

3ag: 4-((methylamino)(phenyl)methyl)benzonitrile

Colorless oil, 60.5% yield. ^{1}H NMR (400 MHz, $CDCl_3$) δ 7.58 (dd, J = 22.0, 8.2 Hz, 4H), 7.34 – 7.31 (m, 4H), 7.29 – 7.22 (m, 1H), 4.75 (s, 1H), 2.42 (s, 3H). ^{1}H NMR data matched the previously reported spectrum.[S17]

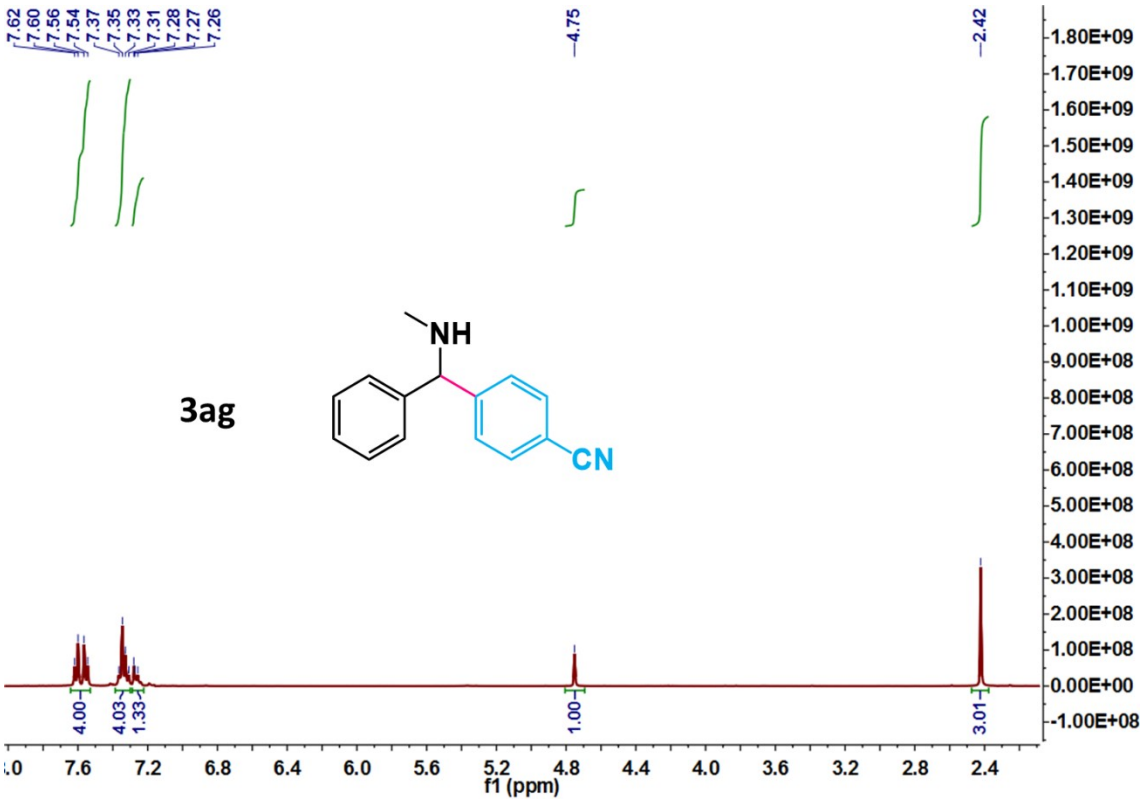

3ah: 4-(morpholino(phenyl)methyl)benzonitrile

Yellowish oil, 44.3% yield. ^{1}H NMR (400 MHz, $CDCl_3$) δ 8.63 (d, J = 2.1 Hz, 1H), 8.50 (dd, J = 1.6, 4.8 Hz, 1H), 7.67 (dt, J = 7.9, 1.9 Hz, 1H), 7.63 (d, J = 7.6 Hz, 2H), 7.55 (d, J = 7.6 Hz, 2H), 7.25 (dd, J = 4.8, 7.8 Hz, 1H), 4.79 (s, 1H), 2.42 (s, 3H). ^{1}H NMR data matched the previously reported spectrum.[S17]

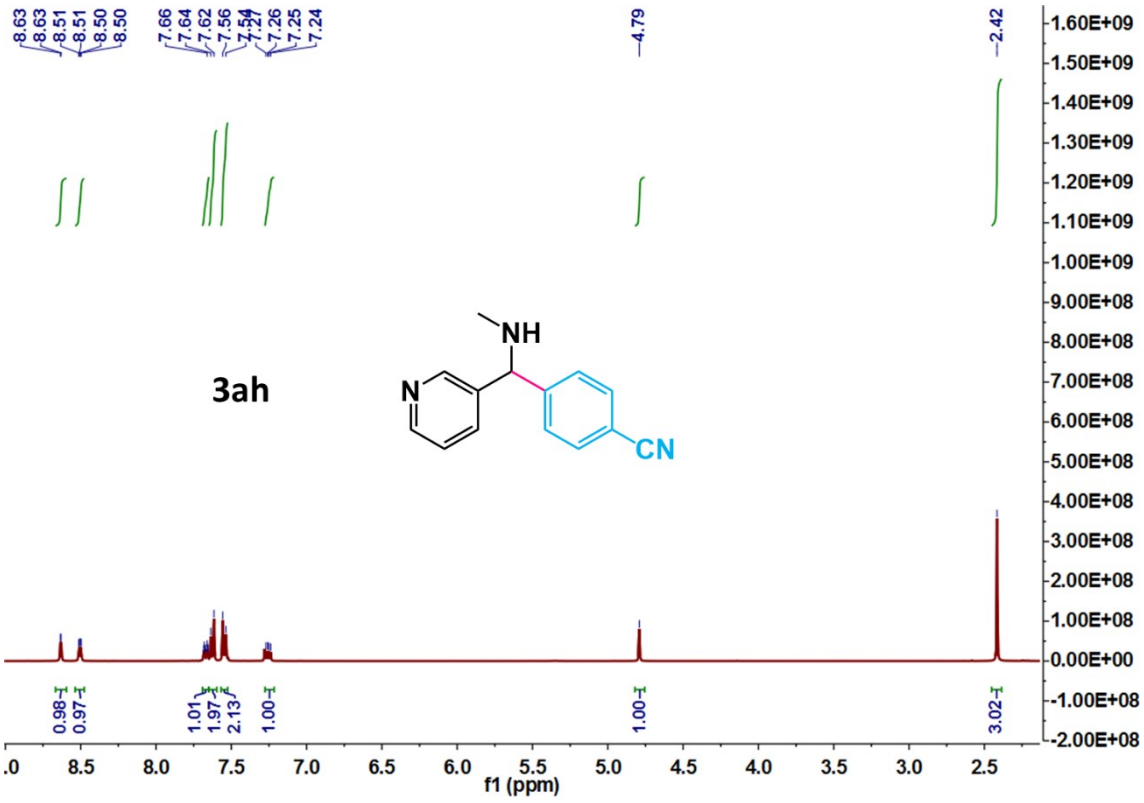

3ai: 4-(morpholino(phenyl)methyl)benzonitrile

Colorless oil, 56.8% yield. ^{1}H NMR (600 MHz, $CDCl_3$) δ 7.49 (s, 4H), 7.30 – 7.26 (m, 2H), 7.23 – 7.19 (m, 2H), 7.16 – 7.12 (m, 1H), 4.19 (s, 1H), 3.64 (t, J = 3.1 Hz 4H), 2.33 – 2.27 (m, 4H). ^{1}H NMR data matched the previously reported spectrum.[S17]

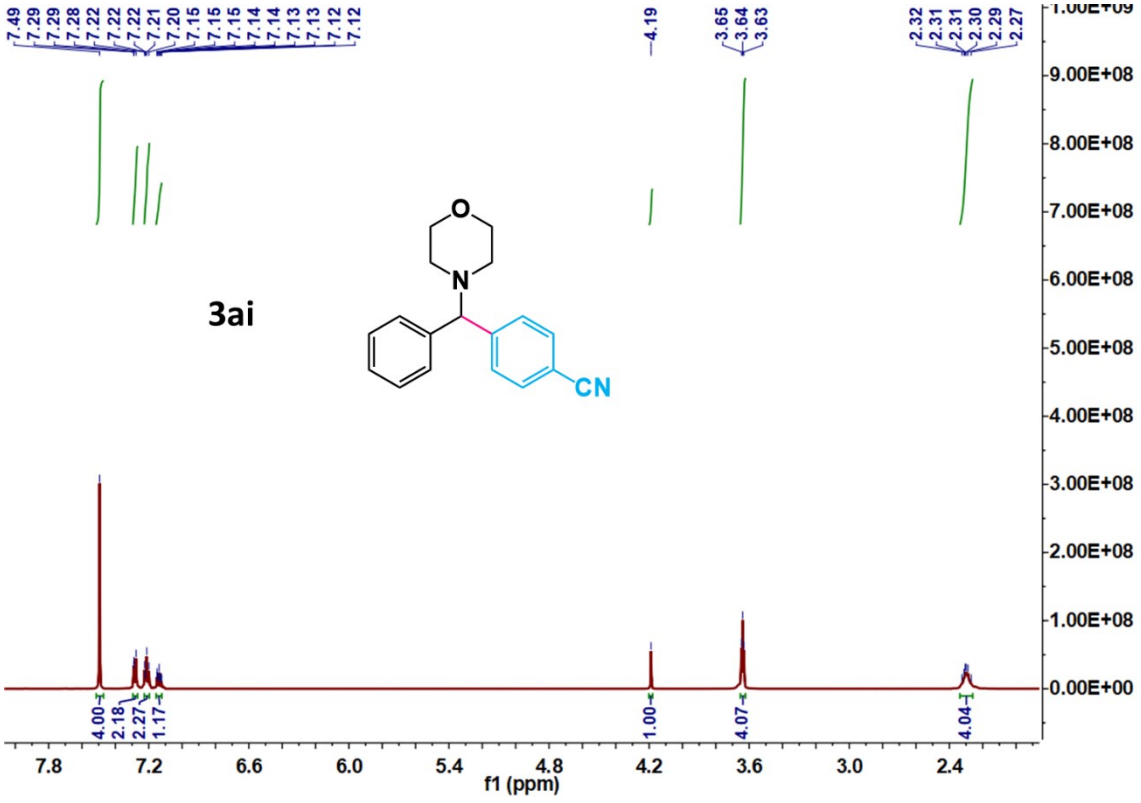

3aj: 4-(phenyl(piperidin-1-yl)methyl)benzonitrile

Colorless oil, 65.2% yield. ^{1}H NMR (400 MHz, $CDCl_3$) δ 7.57 (s, 4H), 7.38 – 7.27 (m, 4H) , 7.23 – 7.14 (m, 1H), 4.30 (s, 1H), 2.32 (s, 4H), 1.59 – 1.54 (m, 4H), 1.42 (d, J = 3.7 Hz, 2H).^{1}H NMR data matched the previously reported spectrum.[S17]

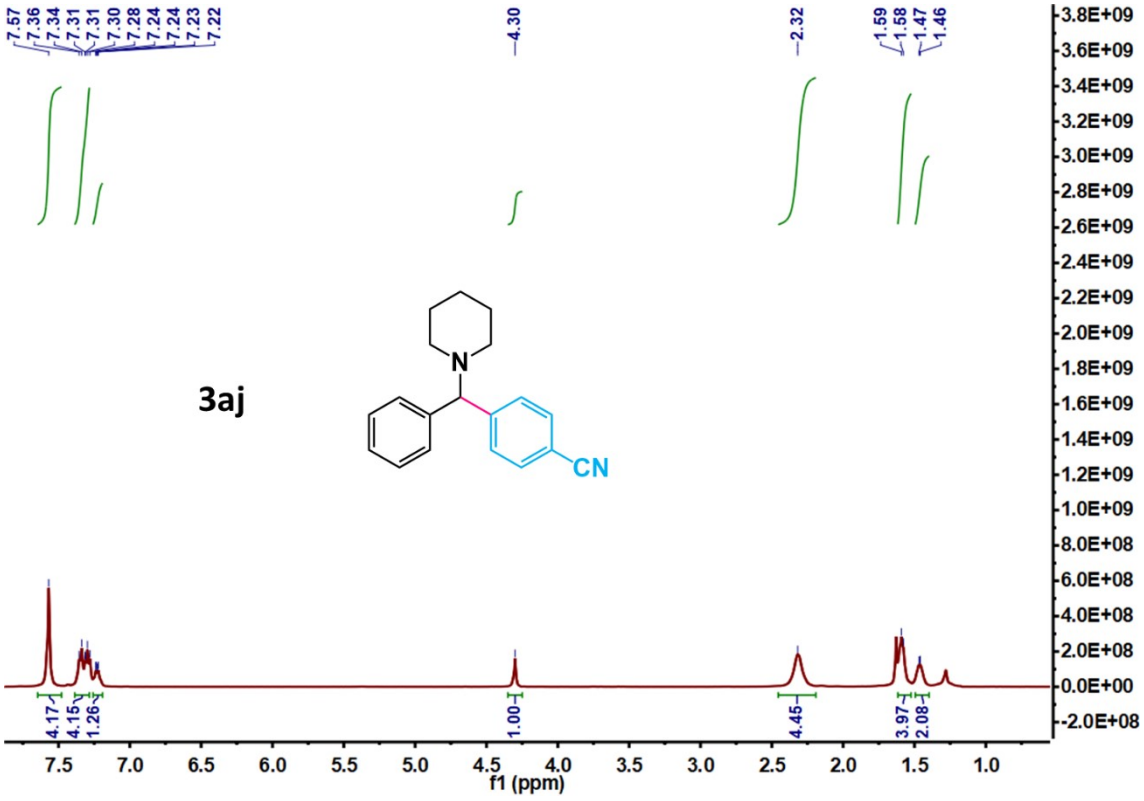

3ak: 4-(phenyl(pyrrolidin-1-yl)methyl)benzonitrile

Colorless oil, 73.1% yield. ^{1}H NMR (400 MHz, $CDCl_3$) δ 7.62 – 7.51 (m, 4H), 7.40 (dd, J = 5.2, 3.4 Hz, 2H), 7.27 (dt, J = 6.2, 2.0 Hz, 2H), 7.23 – 7.16 (m, 1H), 4.21 (s, 1H), 2.39 (dd, J = 5.4, 4.2 Hz, 4H), 1.82 – 1.75 (m, 4H). ^{1}H NMR data matched previously reported spectrum.[S17]

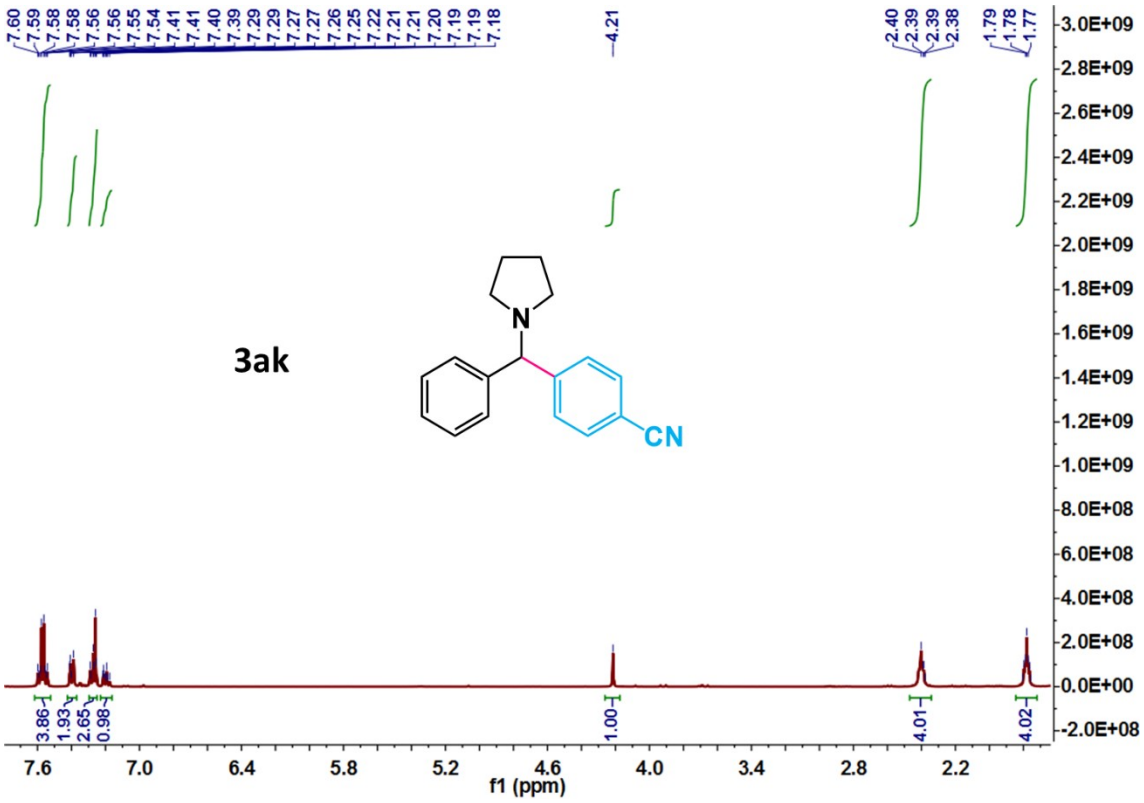

3ck: 2-(phenyl(pyrrolidin-1-yl)methyl)benzonitrile

Colorless oil, 37.8% yield. ^{1}H NMR (400 MHz, $CDCl_3$) δ 7.94 (d, J = 7.8 Hz, 1H), 7.54 (s, 4H), 7.33 – 7.16 (m, 4H), 4.71 (s, 1H), 2.44 (s, 4H), 1.79 (s, 4H). ^{1}H NMR data matched previously reported spectrum.[S16]

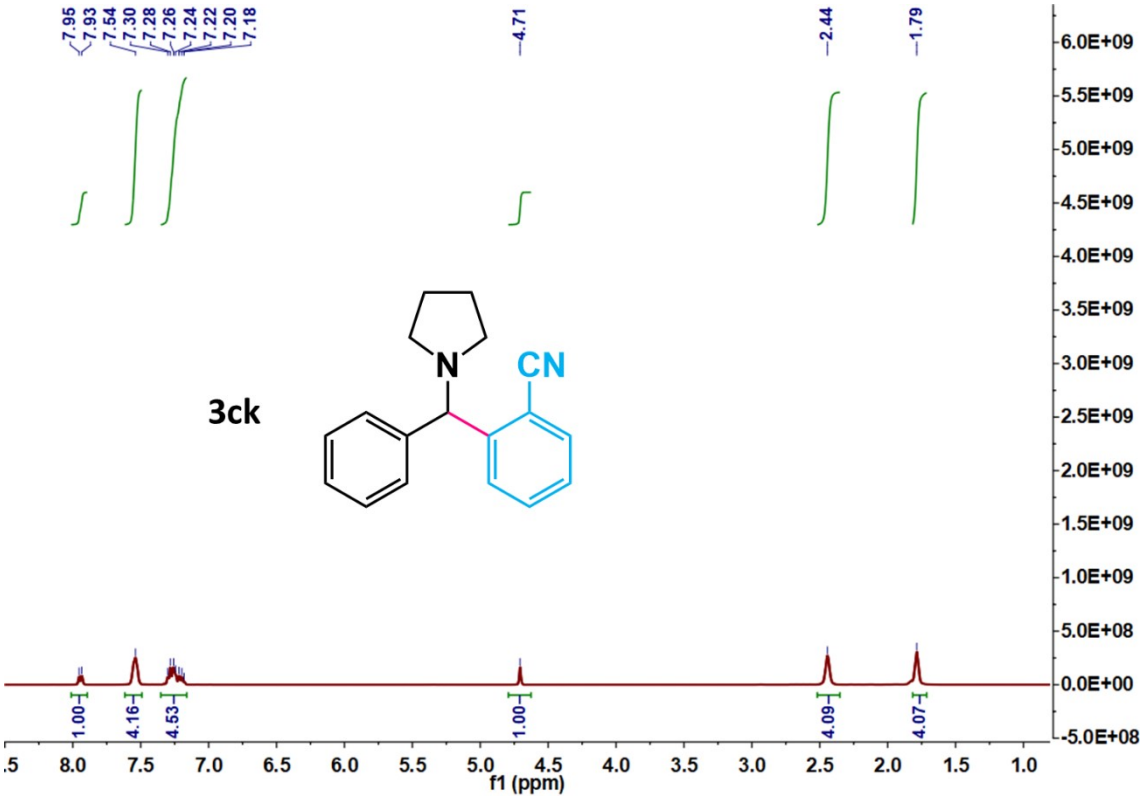

3ek: 4-(phenyl(pyrrolidin-1-yl)methyl)pyridine

Yellowish oil, 46.7% yield. ^{1}H NMR (400 MHz, $CDCl_3$) δ 8.51 (dd, J = 4.5, 1.5 Hz, 2H), 7.46 – 7.39 (m, 4H), 7.31 (d, J = 7.1 Hz, 2H), 7.27 – 7.19 (m, 1H), 4.18 (s, 1H), 2.60 – 2.30 (m, 4H), 1.81 (dd, J = 7.7, 5.5 Hz, 4H). ^{13}C NMR (101 MHz, $CDCl_3$) δ 152.97, 149.94, 142.62, 128.59, 127.58, 127.43, 122.61, 75.42, 53.39, 23.53. HRMS (ESI^+): Calcd. for $[C_{16}H_{18}N_2 + H]^+$: m/z = 239.1543, Found: 239.1547.

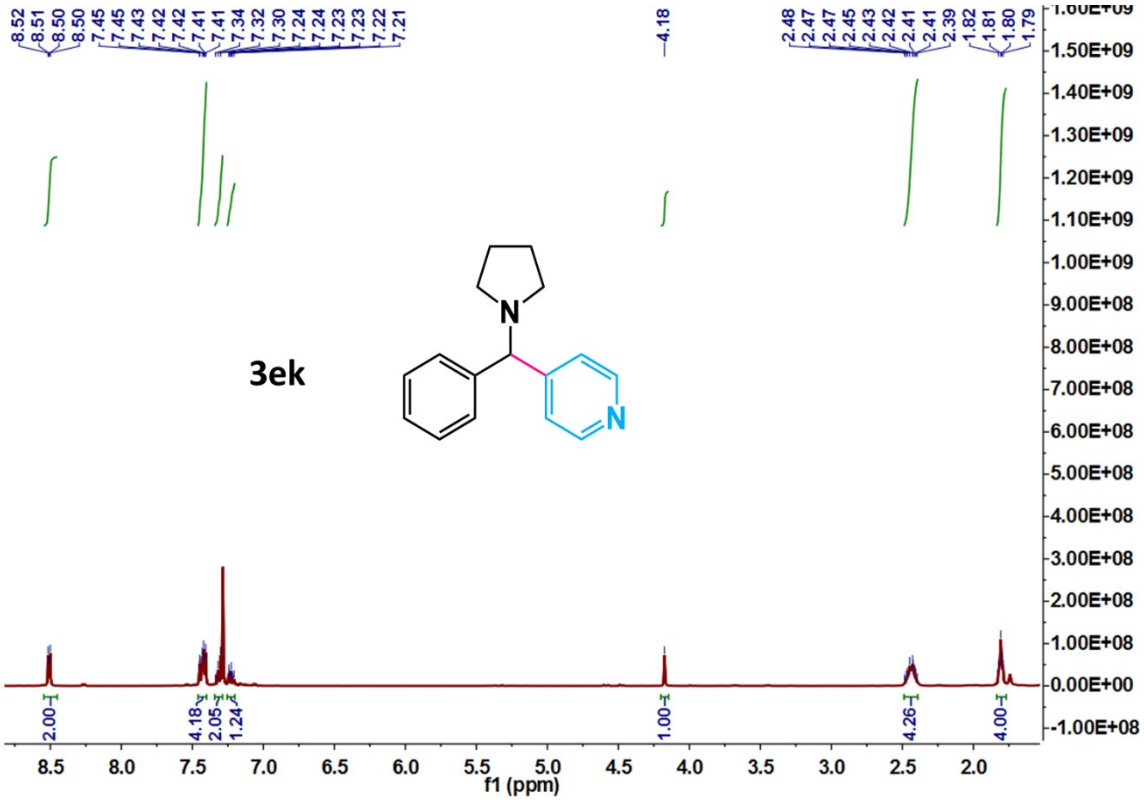

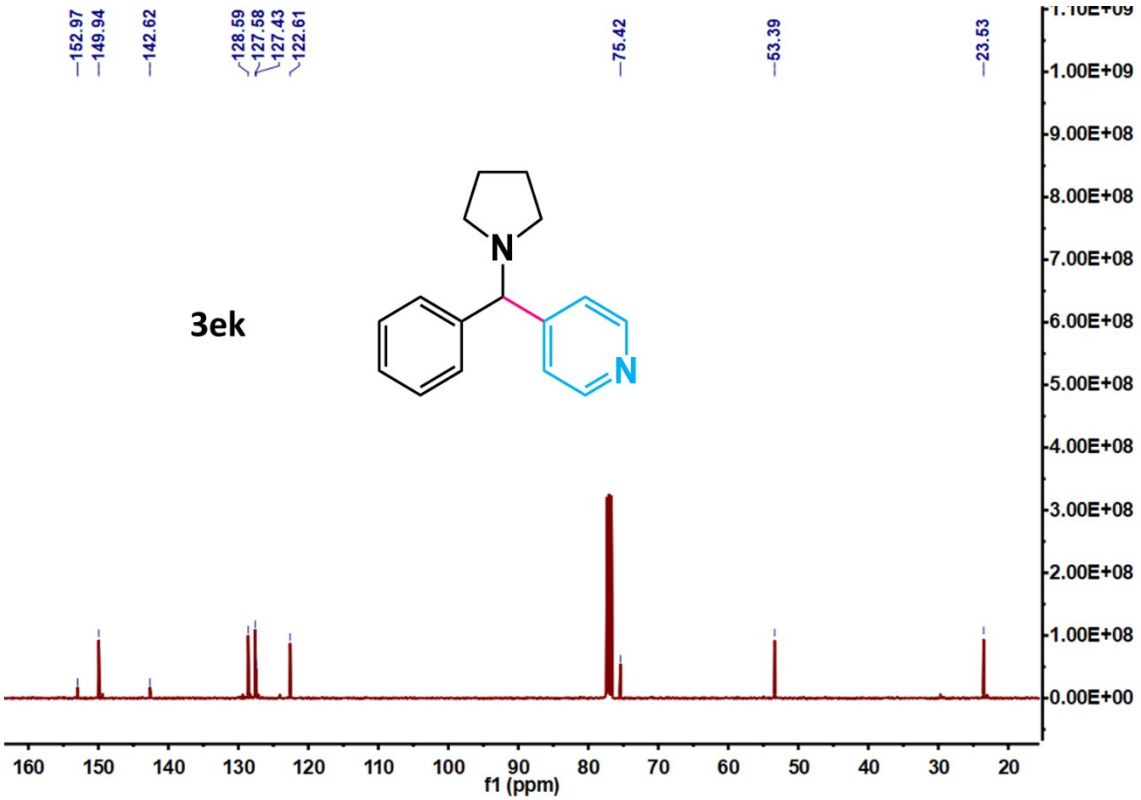
152.97
149.94
142.62
128.59
127.58
127.43
122.61
76.42
53.39
23.53
3ek
N
N
1.00E+09
9.00E+08
8.00E+08
7.00E+08
6.00E+08
5.00E+08
4.00E+08
3.00E+08
2.00E+08
1.00E+08
0.00E+00
160 150 140 130 120 110 100 90 80 70 60 50 40 30 20
f1 (ppm)

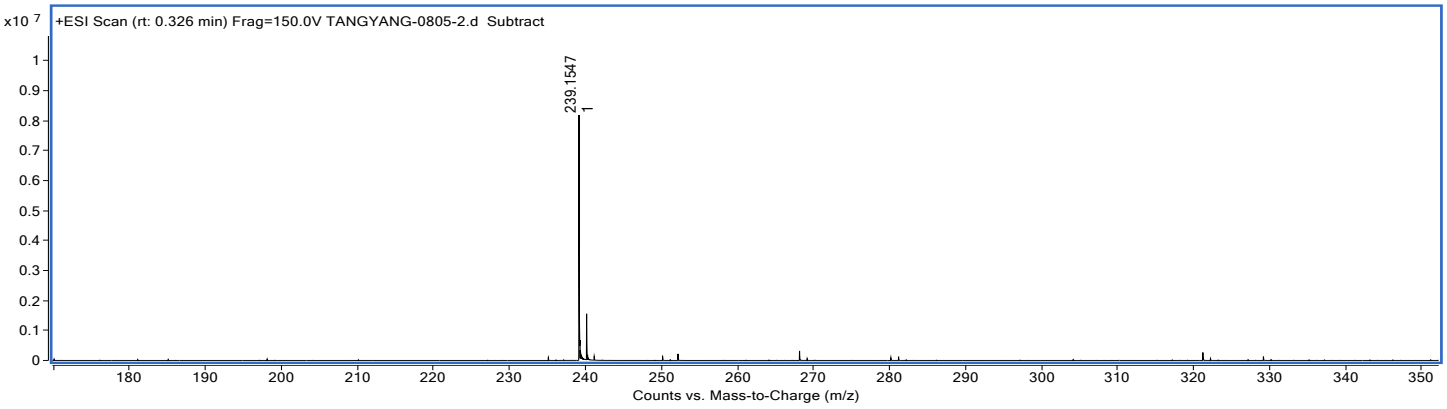
x10 7
+ESI Scan (rt: 0.326 min) Frag=150.0V TANGYANG-0805-2.d Subtract
239.1547
1
1
0.9
0.8
0.7
0.6
0.5
0.4
0.3
0.2
0.1
0
180 190 200 210 220 230 240 250 260 270 280 290 300 310 320 330 340 350
Counts vs. Mass-to-Charge (m/z)

3fk: 2-(phenyl(pyrrolidin-1-yl)methyl)pyridine

Yellow oil, 46.7% yield. ^{1}H NMR (400 MHz, $CDCl_3$) δ 8.52 (d, J = 4.3 Hz, 1H), 7.72 – 7.48 (m, 4H), 7.32 – 7.26 (m, 2H), 7.24 – 7.18 (m, 1H), 7.13 – 7.07 (m, 1H), 4.40 (s, 1H), 2.48 (s, 4H), 1.81 (s, 4H). ^{1}H NMR data matched the previously reported spectrum.[S18]

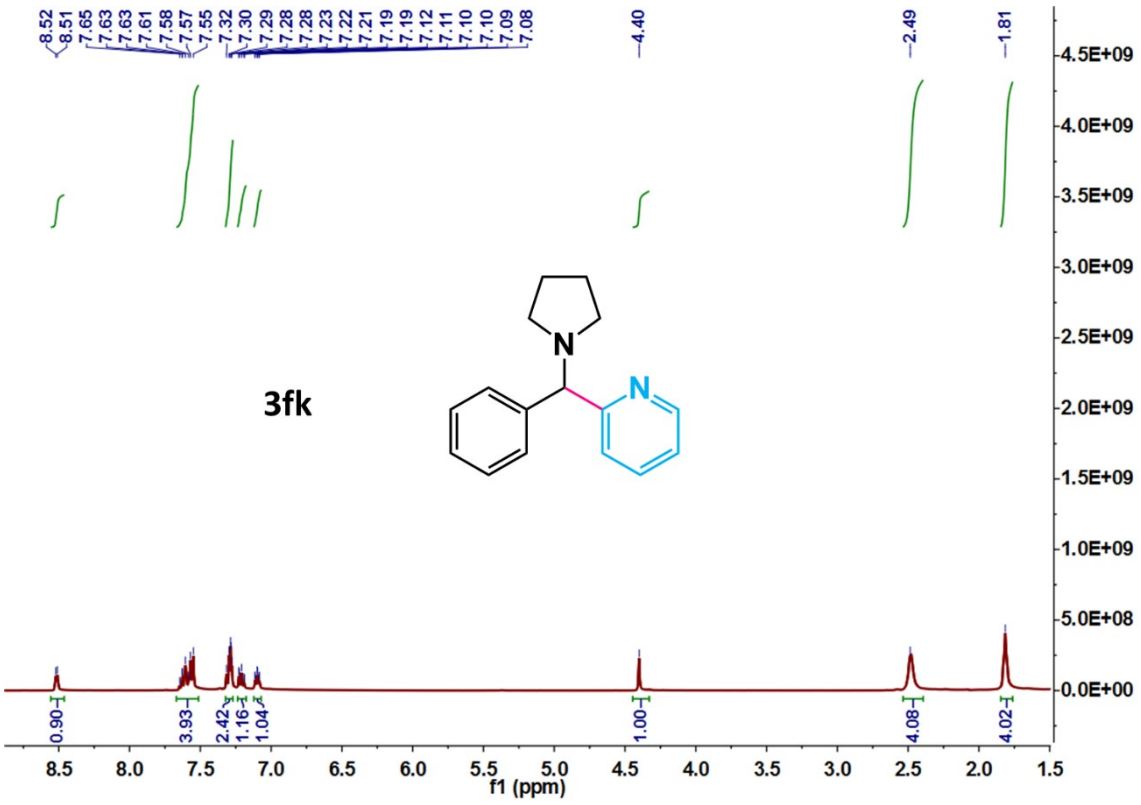

3gk: 2-methyl-4-(phenyl(pyrrolidin-1-yl)methyl)pyridine

Yellow oil, 64.3% yield. ^{1}H NMR (600 MHz, $CDCl_3$) δ 8.29 (d, J = 3.4 Hz, 1H), 7.34 (d, J = 4.8 Hz, 2H), 7.23 – 7.20 (m, 2H), 7.16 (d, J = 3.8 Hz, 1H), 7.15 – 7.11 (m, 2H), 4.03 (s, 1H), 2.43 (s, 3H), 2.39 – 2.29 (m, 4H), 1.71 (s, 4H). ^{13}C NMR (151 MHz, $CDCl_3$) δ 149.23, 142.75, 130.04, 129.75, 128.63, 127.60, 127.44, 122.04, 119.79, 75.61, 53.52, 29.71, 23.54. HRMS (ESI^+): Calcd. for $[C_{17}H_{20}N_2 + H]^+$: m/z = 253.1699, Found: 253.1702.

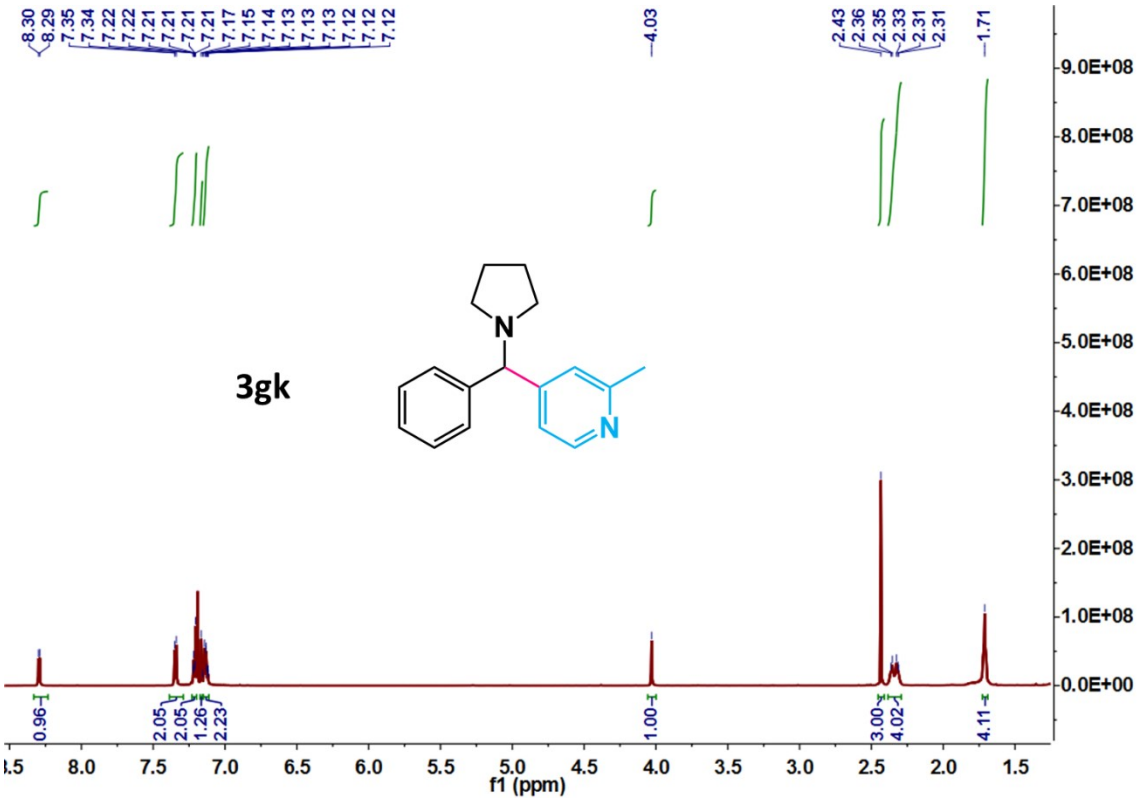

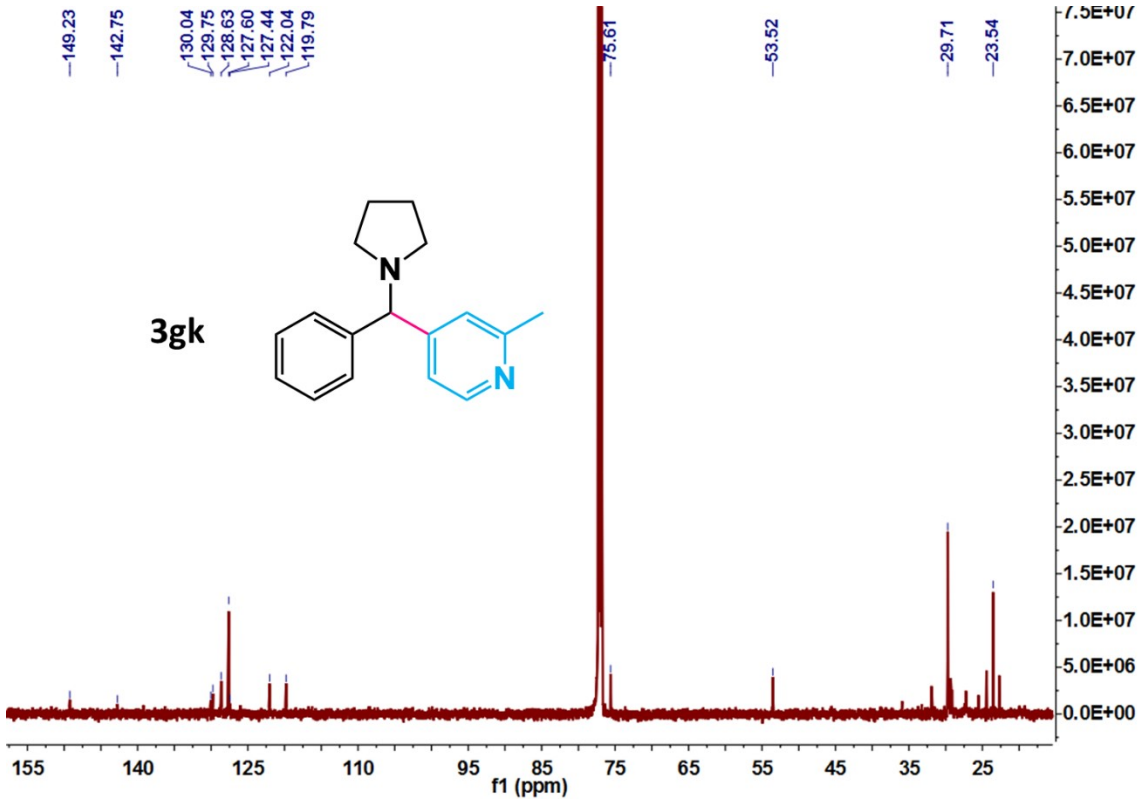
149.23
142.75
130.04
129.75
128.63
127.60
127.44
122.04
119.79
75.61
53.52
29.71
23.54
3gk
N
N
7.5E+07
7.0E+07
6.5E+07
6.0E+07
5.5E+07
5.0E+07
4.5E+07
4.0E+07
3.5E+07
3.0E+07
2.5E+07
2.0E+07
1.5E+07
1.0E+07
5.0E+06
0.0E+00
155
140
125
110
95
85
75
65
55
45
35
25
f1 (ppm)

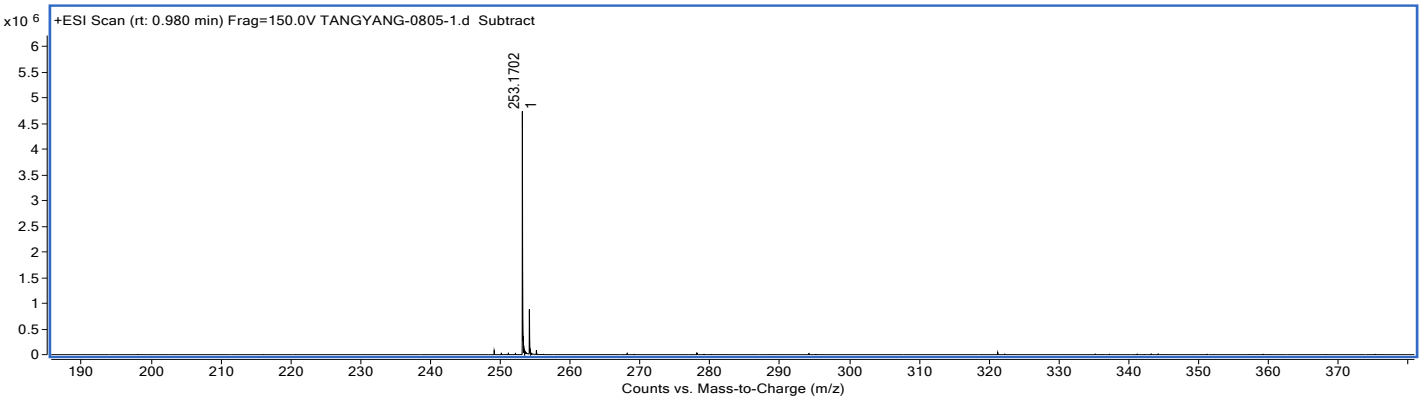
x10 6
+ESI Scan (rt: 0.980 min) Frag=150.0V TANGYANG-0805-1.d Subtract
253.1702
1
6
5.5
5
4.5
4
3.5
3
2.5
2
1.5
1
0.5
0
190
200
210
220
230
240
250
260
270
280
290
300
310
320
330
340
350
360
370
Counts vs. Mass-to-Charge (m/z)

7. References

S1. K. Muralirajan, R. Kancherla and M. Rueping, Dehydrogenative Aromatization and Sulfonylation of Pyrrolidines: Orthogonal Reactivity in Photoredox Catalysis, *Angew. Chem. Int. Ed*., 2018, **57**, 14787–14791.

S2. G. Chen, Y. He, S. Zhang and J. Zhang, Tuning a layer to a three-dimensional cobalt-tris(4′-carboxybiphenyl)amine framework by introducing potassium ions, *Inorganic Chemistry Communications*, 2018, **90**, 65–68.

S3. G. Kresse and J. Furthmuller, Efficiency of ab-initio total energy calculations for metals and semiconductors using a plane-wave basis set, *Comput. Mater. Sci*., 1996, **6**, 15–50.

S4. G. Kresse and J. Furthmuller, Efficient iterative schemes for ab-initio total-energy calculations using a plane-wave basis set. *Phys. Rev. B.*, 1996, **54**, 11169–11186.

S5. P. Hohenberg and W. Kohn, Inhomogeneous electron gas, *Phys. Rev.*, 1964, **136**, 864–871.

S6. W. Kohn and L. Sham, Self-consistent equations including exchange and correlation effects, *Phys. Rev.*, 1965, **140**, 1133–1138.

S7. P. Blöchl, Projector augmented-wave method, *Phys. Rev. B: Condens. Matter.*, 1994, **50**, 17953–17979.

S8. J. Perdew, K. Burke and M. Ernzerhof, Generalized gradient approximation made simple, *Phys. Rev. Lett.*, 1996, **77**, 3865–3868.

S9. Y. Matsuo, Y. Wang, H. Ueno, T. Nakagawa and H. Okada, Mechanochromism, Twisted/Folded Structure Determination, and Derivatization of (*N*-Phenylfluorenylidene)acridane, *Angew. Chem. Int. Ed.*, 2019, **58**, 8762–8767.

S10. SMART Data collection software (version 5.629), Bruker AXS Inc., Madison, WI, 2003.

S11. SAINT, Data reduction software (version 6.45), Bruker AXS Inc., Madison, WI, 2003.

S12. G. Sheldrick, Crystal Structure Refinement with SHELXL, *Acta Crystallogr.*, Sect. C: Struct. Chem., 2015, **71**, 3–8.

S13. Spek, A. Single-crystal structure validation with the program PLATON, *J. Appl. Cryst*. 2003, **36**, 7–13.

S14. Y. Ma, X. Yao, L. Zhang, P. Ni, R. Cheng and J. Ye, Direct Arylation of α-Amino C(sp^3)–H Bonds by Convergent Paired Electrolysis, *Angew. Chem. Int. Ed.*, 2019, **58**, 16548–16552.

S15. C. Xu, F. Shen, G. Feng and J. Jin, Visible-Light-Induced α-Amino C–H Bond Arylation Enabled by Electron Donor–Acceptor Complexes, *Org. Lett*., 2021, **23**, 3913–3918.

S16. H. Li, Y. Yang, X. Jing, C. He and C. Duan, Triarylamine-based porous coordination polymers performing both hydrogen atom transfer and photoredox catalysis for regioselective α-amino C(sp^3)–H arylation, *Chem. Sci*., 2021, **12**, 8512–8520.

S17. T. Ide, J. Barham, M. Fujita, Y. Kawato, H. Egami and Y. Hamashima, Regio- and chemoselective Csp^3–H arylation of benzylamines by single electron transfer/hydrogen atom transfer synergistic catalysis, *Chem. Sci.*, 2018, **9**, 8453–8460.

S18. B. Kim, J. Jiméne, F. Gao, and P. Walsh, Palladium-Catalyzed Benzylic C–H Arylation of Azaarylmethylamines, *Org. Lett*., 2015, **17**, 5788–5791.